COMPUTATIONAL AND EXPERIMENTAL STUDIES OF CHROMIUM-PAH COMPLEXES

by

XIANGJI LIU

(Under the Direction of Michael A. Duncan)

ABSTRACT

A series of Cr-PAH complexes are studied with the size of PAH increasing from benzene to naphthalene, to pyrene, and to coronene. Both the mono-PAH and bis-PAH complexes are studied with density functional theory (DFT). Three typical DFT methods are used in this study, including B3LYP, PBE, and M06L. Geometries, spin states, binding energies, and ionization potentials are investigated theoretically. Cr is found to prefer the binding on the six-member rings with less shared carbons. It may bind to PAHs on either the η_2 or η_6 position. The mono-PAH complexes prefer high spin states, and the bis-PAH complexes prefer low spin states. The trend of binding energies of Cr to these PAHs is not apparent from the calculations. Complexes with larger PAHs have lower ionization potentials. The laser vaporization flowtube reactor (LVFR) is used to synthesize Cr-coronene complexes. The mass spectra indicate these complexes are successfully made in the LVFR.

INDEX WORDS: Polycyclic Aromatic Hydrocarbon Chromium Organometallics DFT Energetics Geometries Laser vaporization

COMPUTATIONAL AND EXPERIMENTAL STUDIES OF CHROMIUM-PAH COMPLEXES

by

XIANGJI LIU
B.S., Wuhan University, 2013

A Dissertation Submitted to the Graduate Faculty of The University of Georgia in Partial Fulfillment of the Requirements for the Degree

DOCTOR OF PHILOSOPHY

ATHENS, GEORGIA
2019

COMPUTATIONAL AND EXPERIMENTAL STUDIES OF CHROMIUM-PAH COMPLEXES

by

XIANGJI LIU

Major Professor:	Michael A. Duncan
Committee:	Tina Salguero
	Gary Douberly

Electronic Version Approved:

Ron Walcott
Interim Dean of the Graduate School
The University of Georgia
December 2019

DEDICATION

I dedicate this dissertation to my dear family, for the fostering and teaching from my parents, for the love from my wife, and for the prayer support from my church family.

ACKNOWLEDGEMENTS

I would like to express my deepest appreciation to Prof. Michael Duncan, who has guided me through the graduate school in the past six years. His rich knowledge is a solid foundation of my research. His contagious enthusiasm about science has encouraged me to work. His accurate scientific criticism has put me in the right track. Without his persistent support, this dissertation would not be possible.

I would also like to give thanks to my co-workers. Scott Akin taught me hand-by-hand to run the apparatus. I also enjoyed working together with Melissa Woodard and Ian Webster in the experiments. Joshua Marks gave me many useful advices for theory calculations. Thanks to the whole Duncan group for keeping my days entertaining.

I am grateful to be in the Department of Chemistry, UGA. My committee members Tina Salguero and Gary Douberly are very helpful, as well as all the other faculties and staff.

Special thanks to my family and friends. They were always accompanying me whether I was in good times or bad. They made all these possible so I get where I am right now.

TABLE OF CONTENTS

Page

LIST OF TABLES

Page

LIST OF FIGURES

Page

CHAPTER 1

BACKGROUND

Transition metals (TMs) have played a vital role in chemistry due to their inherent properties such as diverse valence shell filling probability, catalytic activity and the ability to complex various organic molecules. Some of the most important chemical industrial processes in human history rely on transition metals as catalysts, for instance, the Haber process (Fe), the contact process for producing sulfuric acid (V), the Ostwald process (Pt) and the Fischer-Tropsch process (Co, Fe or Ru). Theoretically, by downsizing the catalyst particles, the atom efficiency of the catalyst can be increased. The smallest particles in chemical reactions are single atoms or single molecules. One of the drawbacks is the high surface energy, which makes them prone to aggregation under realistic reaction conditions.[1–3]

It was not until 2011 that Qiao et al. prepared a Pt single atom catalyst (SAC) anchored on an iron oxide nanocrystalline surface for the first time, and proved its catalytic activity, stability, and selectivity.[4] This demonstrated the possibility of making SACs in the laboratory. Since then, many isolated atoms have been successfully loaded on to carrier surfaces of metal, metal oxide and carbon materials.[3] Among these surfaces, graphene is very intriguing because of its relatively low manufacturing cost and distinct properties. Graphene can be considered as a layer of carbons arranged in a hexagonal honeycomb structure, which is isolated from graphite. It is a two-dimensional (2D) material with a thickness of only an atom.[5] Due to its similarity to graphite, it can be treated as a free-standing graphite surface. An alternative approach is to see graphene as a giant molecule,[5] where it can be treated as an extended array of benzene π systems.

In this scenario, polycyclic aromatic hydrocarbons (PAHs) would be reasonable models of graphene.[6–8]

Polycyclic aromatic hydrocarbons (PAHs) and their derivatives are ubiquitous in environments where carbon is present. They are produced during fuel combustion and some of them are suggested to be carcinogenic.[9,10] The optical properties of PAHs, such as their absorption, fluorescence, and phosphorescence spectroscopies are well documented through gaseous and thin-film studies.[10–12] Ionized PAHs have been proposed as possible carriers of the diffuse interstellar bands (DIBs)[13–20] or the unidentified infrared bands (UIBs).[21,22]

Metal-PAH complexes provide models for metal-graphene catalysts. They are also studied as potential materials for spintronics.[23–25] Additionally in astrophysics, it has been suggested by Serra and co-workers that iron-PAH complexes may exist in the interstellar medium (ISM).[26,27] Metal-PAH complexes have been proposed to exist in the ISM as likely contributors of the DIBs and UIBs.[28,29]

Metal-PAH systems have attracted several groups to produce these species in laboratory experiments. Dunbar and co-workers observed metal-PAH ion complexes in gas-phase experiments using FT-ICR mass spectrometry.[30,31] In this work, they discussed the association kinetics of various metal and non-metal cations with PAHs. Our group has produced a variety of metal and multi-metal complexes with PAHs by laser ablating film-coated metal samples in a molecular beam cluster source.[32–36] Competitive binding and photodissociation successfully determined the relative binding strengths of metal with benzene, coronene, and C_{60}.[34] Photodissociation of $Cr_m(coronene)_n^+$ complexes confirmed the formation of multi-metal and multidecker sandwich structures.[32] Photoelectron spectroscopy of complexes with vanadium and

two coronenes suggested that the metal may bind between the molecules as in a sandwich, or also to the external side of a PAH dimer complex.[36] Similar complexes were also produced by other methods without the supersonic expansion cooling.[37–39] This indicated that some metal-PAH complexes are bound strongly enough to survive the hot conditions in these experiments. Eyler and co-workers observed the infrared spectra of complexes of Fe^+ and PAHs in a Fourier transform ion cyclotron resonance (FT-ICR) mass spectrometer.[39]

Theoretical methods have also been used to study metal-PAH complexes. Some early investigations were conducted by Dunbar,[40] Klippenstein and co-workers,[41] Eyler and co-workers,[39] and Jena and co-workers.[42,43] Klippenstein and co-workers suggested that the metal ion-coronene bond strength is comparable to its metal-benzene counterpart,[41] which is consistent with our experimental estimates.[34] As theoretical methods and computers have developed in the past years, more recent studies about metal-PAH complexes have been published.[44–47]

Many combinations of TMs and π ligands are possible. However, this study focuses only on complexes with chromium (Cr) atoms. Cr is known to form stable complexes with benzene such as bis(benzene)chromium.[48] It is therefore likely that Cr complexes with other ligands having benzene-like structures, including coronene and graphene, are also stable. Therefore, the theoretical study of Cr-π complexes may be compared to experimental results either for small ligands now or for larger ligands such as coronene and graphene in the future. To study the effects of sizes of π conjugated systems, ligands of different sizes from benzene to naphthalene, to pyrene, and to coronene are chosen. Because of the computational cost of our calculations, the largest ligand used in this study is coronene.

References

(1) Uzun, A.; Ortalan, V.; Hao, Y.; Browning, N. D.; Gates, B. C. Nanoclusters of Gold on a High-Area Support: Almost Uniform Nanoclusters Imaged by Scanning Transmission Electron Microscopy. *ACS Nano* **2009**, *3*, 3691–3695.

(2) Uzun, A.; Ortalan, V.; Browning, N. D.; Gates, B. C. A Site-Isolated Mononuclear Iridium Complex Catalyst Supported on MgO: Characterization by Spectroscopy and Aberration-Corrected Scanning Transmission Electron Microscopy. *J. Catal.* **2010**, *269*, 318–328.

(3) Yang, X.-F.; Wang, A.; Qiao, B.; Li, J.; Liu, J.; Zhang, T. Single-Atom Catalysts: A New Frontier in Heterogeneous Catalysis. *Acc. Chem. Res.* **2013**, *46*, 1740–1748.

(4) Qiao, B.; Wang, A.; Yang, X.; Allard, L. F.; Jiang, Z.; Cui, Y.; Liu, J.; Li, J.; Zhang, T. Single-Atom Catalysis of CO Oxidation Using Pt_1/FeO_x. *Nat. Chem.* **2011**, *3*, 634–641.

(5) Geim, A. K. Graphene: Status and Prospects. *Science* **2009**, *324*, 1530–1534.

(6) Whittingham, M. S.; Jacobson, A. J. *Intercalation Chemistry*; Academic Press, 1982.

(7) Dresselhaus, M. S.; Dresselhaus, G.; Eklund, P. C. *Science of Fullerenes and Carbon Nanotubes: Their Properties and Applications*; Elsevier Science, 1996.

(8) Enoki, T.; Suzuki, M.; Endo, M. *Graphite Intercalation Compounds and Applications*; Oxford University Press, 2003.

(9) Committee on Pyrene and Selected Analogues; Board on Toxicology and Environmental Health Hazards; Commission on Life Sciences; National Research Council. *Polycyclic Aromatic Hydrocarbons*; National Academies Press: Washington, D.C., 1983.

(10) Harvey, R. G. *Polycyclic Aromatic Hydrocarbons: Chemistry and Carcinogenicity*; Cambridge Monographs on Cancer Research; Cambridge University Press, 1991.

(11) Birks, J. B. *Photophysics of Aromatic Molecules*; Studies in the History of American Education Series; Wiley-Interscience, 1970.

(12) Klessinger, M.; Michl, J. *Excited States and Photochemistry of Organic Molecules*; VCH, 1995.

(13) Bohme, D. K. PAH [Polycyclic Aromatic Hydrocarbons] and Fullerene Ions and Ion/Molecule Reactions in Interstellar and Circumstellar Chemistry. *Chem. Rev.* **1992**, *92*, 1487–1508.

(14) Salama, F.; Bakes, E. L. O.; Allamandola, L. J.; Tielens, A. G. G. M. Assessment of the Polycyclic Aromatic Hydrocarbon--Diffuse Interstellar Band Proposal. *Astrophys. J.* **1996**, *458*, 621.

(15) Hartquist, T. W.; Williams, D. A. *The Molecular Astrophysics of Stars and Galaxies*; International Series on Astron; Clarendon Press, 1998.

(16) Henning, T.; Salama, F. Carbon in the Universe. *Science* **1998**, *282*, 2204–2210.

(17) Bréchignac, P.; Pino, T.; Boudin, N. Laboratory Spectra of Cold Gas Phase Polycyclic Aromatic Hydrocarbon Cations, and Their Possible Relation to the Diffuse Interstellar Bands. *Spectrochim. Acta - Part A Mol. Biomol. Spectrosc.* **2001**, *57*, 745–756.

(18) Tielens, A. G. G. M. *The Physics and Chemistry of the Interstellar Medium*; Cambridge University Press, 2005.

(19) Tielens, A. G. G. M. Interstellar Polycyclic Aromatic Hydrocarbon Molecules. *Annu. Rev. Astron. Astrophys.* **2008**, *46*, 289–337.

(20) Tielens, A. G. G. M.; Snow, T. P. *The Diffuse Interstellar Bands*; Astrophysics and Space Science Library; Springer Netherlands, 2012.

(21) Allamandola, L. J.; Tielens, G. G. M.; Barker, J. R. Interstellar Polycyclic Aromatic

Hydrocarbons - the Infrared Emission Bands, the Excitation/Emission Mechanism, and the Astrophysical Implications. *Astrophys. J. Suppl. Ser.* **1989**, *71*, 733.

(22) Leger, A.; D'Hendecourt, L.; Defourneau, D. Physics of IR Emission by Interstellar PAH Molecules. *Astron. Astrophys.* **1989**, *216*, 148–164.

(23) Wolf, S. A.; Awschalom, D. D.; Buhrman, R. A.; Daughton, J. M.; von Molnár, S.; Roukes, M. L.; Chtchelkanova, A. Y.; Treger, D. M. Spintronics: A Spin-Based Electronics Vision for the Future. *Science* **2001**, *294*, 1488–1495.

(24) Žutić, I.; Fabian, J.; Das Sarma, S. Spintronics: Fundamentals and Applications. *Rev. Mod. Phys.* **2004**, *76*, 323–410.

(25) Maslyuk, V. V.; Bagrets, A.; Meded, V.; Arnold, A.; Evers, F.; Brandbyge, M.; Bredow, T.; Mertig, I. Organometallic Benzene-Vanadium Wire: A One-Dimensional Half-Metallic Ferromagnet. *Phys. Rev. Lett.* **2006**, *97*, 097201.

(26) Chaudret, B.; Lebeuze, A.; Rabaa, H.; Saillard, J. Y.; Serra, G. Organometallic Chemistry in the Interstellar-Medium .2. Theoretical-Study of the Coordination of Iron to Polycyclic-Hydrocarbons. *New J. Chem.* **1991**, *15*, 791–794.

(27) Serra, G.; Chaudret, B.; Saillard, Y.; Lebeuze, A.; Rabaa, H.; Ristorcelli, I.; Klotz, A. Organometallic Chemistry in the Interstellar-Medium .1. Are Organometallic Reactions Efficient Processes in Astrochemistry. *Astron. Astrophys.* **1992**, *260*, 489–493.

(28) Klotz, A.; Marty, P.; Boissel, P.; de Caro, D.; Serra, G.; Mascetti, J.; de Parseval, P.; Derouault, J.; Daudey, J.-P.; Chaudret, B. Possible Contribution of Organometallic Species in the Solar System Ices. Reactivity and Spectroscopy. *Planet. Space Sci.* **1996**, *44*, 957–965.

(29) Caraiman, D.; Bohme, D. K. The Gas-Phase Chemistry of Iron Cations Coordinated to

Benzene and the Extended Aromatic Coronene. *Int. J. Mass Spectrom.* **2003**, *223*, 411–425.

(30) Dunbar, R. C.; Uechi, G. T.; Asamoto, B. Radiative Association Reactions of Silicon and Transition-Metal Cations with the PAH Compounds Benzene, Naphthalene, and Anthracene. *J. Am. Chem. Soc.* **1994**, *116*, 2466–2470.

(31) Pozniak, B. P.; Dunbar, R. C. Monomer and Dimer Complexes of Coronene with Atomic Ions. *J. Am. Chem. Soc.* **1997**, *119*, 10439–10445.

(32) Foster, N. R.; Grieves, G. A.; Buchanan, J. W.; Flynn, N. D.; Duncan, M. A. Growth and Photodissociation of Cr_x-$(Coronene)_y$ Complexes. *J. Phys. Chem. A* **2000**, *104*, 11055–11062.

(33) Buchanan, J. W.; Reddic, J. E.; Grieves, G. A.; Duncan, M. A. Metal and Multimetal Complexes with Polyaromatic Hydrocarbons: Formation and Photodissociation of Fe_x-$(Coronene)_y$ Cations. *J. Phys. Chem. A* **1998**, *102*, 6390–6394.

(34) Buchanan, J. W.; Grieves, G. A.; Reddic, J. E.; Duncan, M. A. Novel Mixed Ligand Sandwich Complexes: Competitive Binding of Iron with Benzene, Coronene, and C_{60}. *Int. J. Mass Spectrom.* **1999**, *182–183*, 323–333.

(35) Foster, N. R.; Buchanan, J. W.; Flynn, N. D.; Duncan, M. A. Ring Destruction and Carbide Formation in Niobium-PAH Complexes. *Chem. Phys. Lett.* **2001**, *341*, 476–482.

(36) Duncan, M. A.; Knight, A. M.; Negishi, Y.; Nagao, S.; Judai, K.; Nakajima, A.; Kaya, K. Photoelectron Spectroscopy of $V_x(Coronene)_y$ and $Ti_x(Coronene)_y$ Anions. *J. Phys. Chem. A* **2001**, *105*, 10093–10097.

(37) Ayers, T. M.; Westlake, B. C.; Duncan, M. A. Laser Plasma Production of Metal and Metal Compound Complexes with Polycyclic Aromatic Hydrocarbons. *J. Phys. Chem. A*

2004, *108*, 9805–9813.

(38) Ayers, T. M.; Westlake, B. C.; Preda, D. V.; Scott, L. T.; Duncan, M. A. Laser Plasma Production of Metal−Corannulene Ion−Molecule Complexes. *Organometallics* **2005**, *24*, 4573–4578.

(39) Szczepanski, J.; Wang, H.; Vala, M.; Tielens, A. G. G. M.; Eyler, J. R.; Oomens, J. Infrared Spectroscopy of Gas-Phase Complexes of Fe^+ and Polycyclic Aromatic Hydrocarbon Molecules. *Astrophys. J.* **2006**, *646*, 666–680.

(40) Dunbar, R. C. Binding of Transition-Metal Ions to Curved π Surfaces: Corannulene and Coronene. *J. Phys. Chem. A* **2002**, *106*, 9809–9819.

(41) Klippenstein, S. J.; Yang, C.-N. Density Functional Theory Predictions for the Binding of Transition Metal Cations to Pi Systems: From Acetylene to Coronene and Tribenzocyclyne. *Int. J. Mass Spectrom.* **2000**, *201*, 253–267.

(42) Senapati, L.; Nayak, S. K.; Rao, B. K.; Jena, P. Atomic Structure, Binding Energy, and Magnetic Properties of Iron Atoms Supported on a Polyaromatic Hydrocarbon. *J. Chem. Phys.* **2003**, *118*, 8671–8680.

(43) Kandalam, A. K.; Kiran, B.; Jena, P.; Li, X.; Grubisic, A.; Bowen, K. H. Ground State Structures and Photoelectron Spectroscopy of $[Co_m(Coronene)]^-$ Complexes. *J. Chem. Phys.* **2007**, *126*, 084306.

(44) Simon, A.; Rapacioli, M.; Lanza, M.; Joalland, B.; Spiegelman, F. Molecular Dynamics Simulations on $[FePAH]^+$ π-Complexes of Astrophysical Interest: Anharmonic Infrared Spectroscopy. *Phys. Chem. Chem. Phys.* **2011**, *13*, 3359.

(45) Lao, K. U.; Tsou, P. K.; Lankau, T.; Yu, C. H. A Computational Study of Organic Polyradicals Stabilized by Chromium Atoms. *Phys. Chem. Chem. Phys.* **2012**, *14*, 138–

147.

(46) Ding, L.-P.; Kuang, X.-Y.; Shao, P.; Zhong, M.-M. Evolution of Structure and Properties of Neutral and Negatively Charged Transition Metal–Coronene Complexes: A Comprehensive Analysis. *Dalt. Trans.* **2013**, *42*, 8644.

(47) Stella, M.; Bennie, S. J.; Manby, F. R. Computational Study of Adsorption of Cobalt on Benzene and Coronene. *Mol. Phys.* **2015**, *113*, 1858–1864.

(48) Fischer, E. O.; Hafner, W. Di-Benzol-Chrom. *Zeitschrift für Naturforsch.* **1955**, *10b*, 665–668.

CHAPTER 2

METHODS

DFT Method

Density functional theory (DFT) has its drawbacks because it uses approximations to describe exchange and correlation interactions. The accuracy of DFT calculations is determined by the quality of exchange-correlation functionals. However, given its generally good accuracy and attractive low cost, DFT remains the most popular choice for the modeling of large organometallic complexes.

Because of the dependence of DFT accuracy on the exchange-correlation (EX) functional, This study uses three mainstream functionals, namely M06-L[1], PBE[2], and B3LYP[3,4]. M06-L uses local density approximation (LDA) for its EX functional, while PBE uses generalized gradient approximations (GGA) for its EX functional. B3LYP is a hybrid functional, which mixes approximate and exact EX functionals. The default percentage of the exact HF exchange in B3LYP set by common quantum chemistry software packages is 20%. On the Jacob's ladder of approximations, hybrid functionals are of a higher rung than GGA, and LDA is on the lowest rung.[5,6] According to this, the hybrid functional B3LYP is theoretically a better method. However, previous studies have shown that approximate exchange functionals tend to overstablize low spin states, and having HF exchange in the functional overstablizes high spin states.[7,8] Moreover, without comparison to experimental data, it is difficult to determine the best HF exchange percentage for a specific molecular system. On the other hand, M06-L is the

newest functional among the three and is optimized for transitional metal complexes. After all, none of the functionals is guaranteed to give better results than the others, unless tested by experiments. The basis set used with all three DFT methods is def2-TZVP.[9]

There are many quantum chemistry (QC) software packages available now. Gaussian 09 or Gaussian 16 may be the most used package by researchers around the world. Among the free QC software packages, ORCA[10] is probably the most popular one for DFT calculations, and it is used for all the theory calculations in the following chapters.

Some useful features included in ORCA are applied in this study. Considering that these clusters have as many as 73 atoms, the resolution-of-identity (RI) approximation RIJCOSX was applied to accelerate self-consistent field (SCF) calculations.[11] Otherwise, it is almost impossible to apply this level of theory to all the following calculations, especially the Cr-Coronene complexes. The auxiliary basis def2/J is used by RIJCOSX.[12] Traditional DFT methods like B3LYP and PBE cannot describe dispersion forces, and have to be corrected to obtain accurate energies. Therefore the DFT-D3 correction is applied to all the calculations in this study.[13,14] Because weak interactions are involved in some of the clusters studied, this work uses the geometrical counterpoise correction (gCP) to correct for the basis set superposition error (BSSE).[15]

Properties from Theory

Structures and energetics of the target complexes are derived from the theory results, including the positions of Cr atoms relative to PAH molecules, the spin states, binding energies, and ionization potentials.

PAH molecules that have multiple fused benzene rings and provide multiple binding sites for the Cr atom to interact with. When studying $Cr(PAH)_1$ complexes, relaxed geometry optimizations are started with Cr binding to each possible η^2 or η^6 site of the PAH. If the structures end with Cr sitting directly above a carbon atom, they are named after the closest η^2 sites, since the metal atom will lean in one direction or another. For $Cr(PAH)_2$ sandwich complexes, only η^6 sites are considered to bind Cr. Details of the model setup for each specific PAH complex are discussed later in the corresponding chapters.

A bare Cr atom has the electronic configuration of $[Ar]3d^5 4s^1$. This gives rise to several possible spin multiplicities (represented by M=2S+1) for the Cr-PAH complexes. A neutral complex with a single Cr can be a singlet (M=1), triplet (M=3), quintet (M=5), or septet (M=7). A singly-charged cationic complex can be a doublet (M=2), quartet (M=4), or sextet (M=6). Geometry optimizations are performed for all of the possible spin multiplicities for each complex. Energy differences between every spin state are compared to determine the ground spin states.

Three kinds of binding energies are derived. *B.E.1* stands for the binding energy between a bare Cr atom or ion and a PAH molecule. *B.E.2* is calculated by subtracting the energy of a $Cr(PAH)_2$ complex from the sum of energies of a $Cr(PAH)_1$ complex and a PAH molecule. *B.E.sum* is the energy needed by a Cr atom or ion binding with two PAH molecules to form the $Cr(PAH)_2$ complex. Considering that the number of ligands around the metal may affect the spin multiplicity of the complex, binding energies are calculated with and without spin cross over.

Adiabatic and vertical ionization potentials are calculated. The adiabatic ionization potentials are obtained by subtracting the lowest energy of a neutral complex from the lowest energy of the corresponding cation. To obtain vertical ionization potentials, single point energies of cations

are calculated using the geometries optimized for neutral complexes. The spin multiplicities of the cations are restricted by $\Delta M=\pm 1$. This limits the vertical ionization process to the loss of one electron without electron rearrangements.

Experiment Setup

Metal PAH complex syntheses are attempted in a home-made apparatus called the Laser Vaporization Flowtube Reactor (LVFR). The design of the apparatus was developed from ideas first described by Andres and co-workers.[16–18] The LVFR was described in detail previously.[19,20] In this setup, we employ laser vaporization for the metals. PAHs were sublimed from a heated oven.

The schematic of the LVFR is shown in Figure 2.1. The apparatus has three sections connected in one vacuum chamber: vaporization, cooling, and collection. In the vaporization section, the rotating metal rod is ablated by a laser to create a plasma. An excimer laser (Coherent LPX Pro 240F, KrF, 248 nm) running at high power (90-120 mJ/pulse) and high repetition rate (400 Hz) is used to ablate the metal rod. PAH vapors are produced using a ceramic oven wrapped by a nickel-chromium alloy resistance heating wire which is placed beside the metal rod. The oven's mouth is facing the metal rod, and its temperature is monitored by a thermocouple gauge. The PAH vapor and metal plasma are both entrained in a flow of inert carrier gas, where metal atoms and PAH vapors interact with each other and form metal-PAH clusters. The cooling of hot vapors happens through collisions with the carrier gas. The wall of the first chamber is cooled by chilled water.

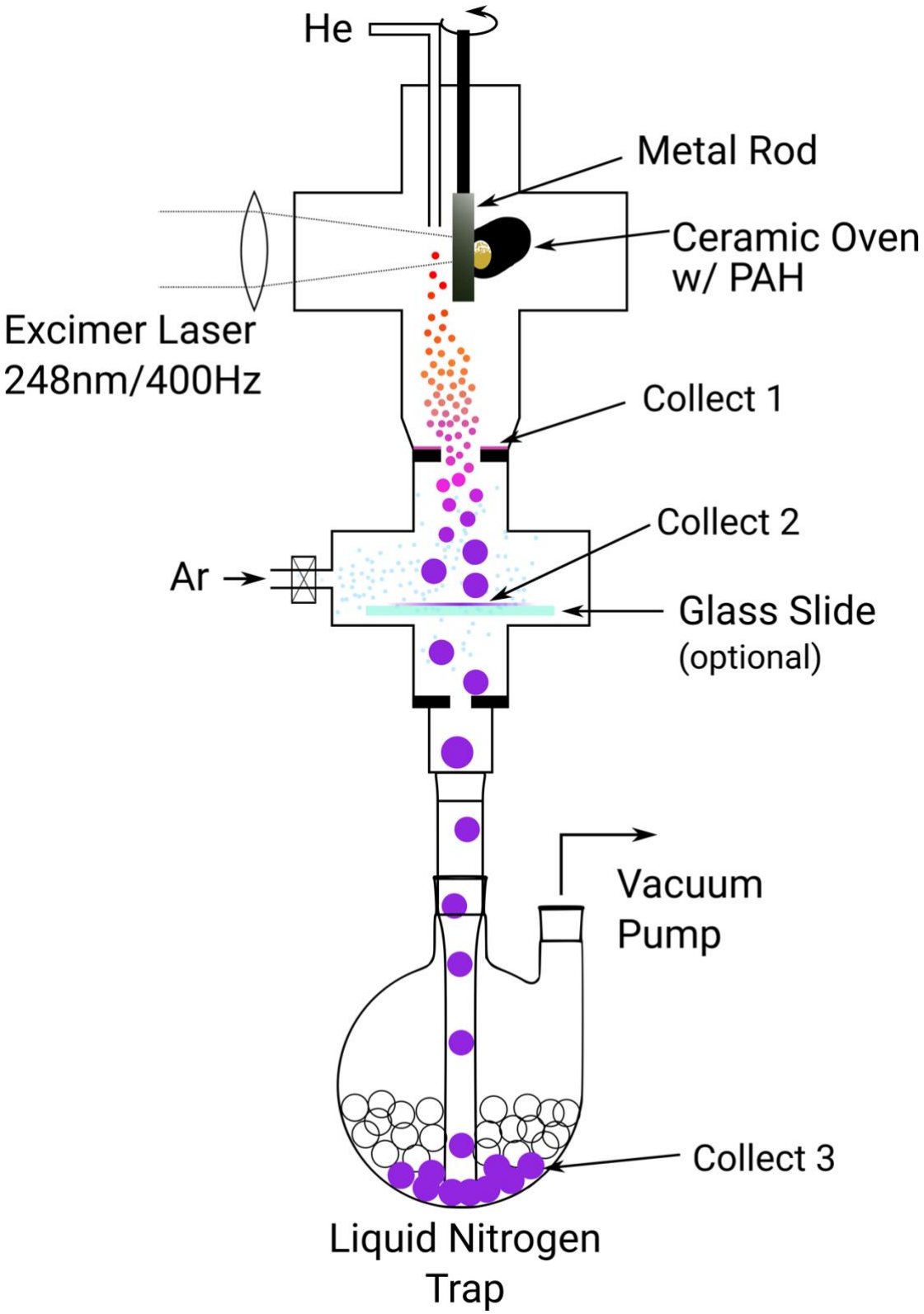

Figure 2.1 The schematic of the laser vaporization flowtube reactor (LVFR).

Clusters move down the flowtube into the second chamber through a 13 mm aperture. This aperture slows the gas flow, thus promoting collisional cooling of the clusters. Additional argon gas is introduced into this chamber to provide additional collisional cooling. A solvent can also be added here if materials in solution are wanted.

Materials are collected at several positions in the flow tube. The first is the upper side of the 13 mm aperture. The second position is at the crossing point into the second chamber, where a glass collection slide is inserted into the gas flow. The last position is in the round bottom flask, which is filled to an approximate depth of 50 mm with 5 mm diameter glass beads. This flask can be cooled by liquid nitrogen. The gaseous materials flow down into the flask through a 7 mm aperture. This aperture restricts the flow rate to increase collisions of materials in the second chamber.

The system is evacuated by an Edwards E2M40 mechanical pump to an ultimate pressure of 1×10^{-3} torr. Two liquid nitrogen traps are used in between the pump and the collecting flask to prevent back-streaming of oil into the sample as well as organic solvents into the pump.

References

(1) Zhao, Y.; Truhlar, D. G. A New Local Density Functional for Main-Group Thermochemistry, Transition Metal Bonding, Thermochemical Kinetics, and Noncovalent Interactions. *J. Chem. Phys.* **2006**, *125*, 194101.

(2) Perdew, J. P.; Burke, K.; Ernzerhof, M. Generalized Gradient Approximation Made Simple. *Phys. Rev. Lett.* **1996**, *77*, 3865–3868.

(3) Becke, A. D. Density-Functional Thermochemistry. III. The Role of Exact Exchange. *J. Chem. Phys.* **1993**, *98*, 5648–5652.

(4) Stephens, P. J.; Devlin, F. J.; Chabalowski, C. F.; Frisch, M. J. Ab Initio Calculation of Vibrational Absorption and Circular Dichroism Spectra Using Density Functional Force Fields. *J. Phys. Chem.* **1994**, *98*, 11623–11627.

(5) Perdew, J. P. Jacob's Ladder of Density Functional Approximations for the Exchange-Correlation Energy. In *AIP Conference Proceedings*; 2001.

(6) Perdew, J. P.; Ruzsinszky, A.; Tao, J.; Staroverov, V. N.; Scuseria, G. E.; Csonka, G. I. Prescription for the Design and Selection of Density Functional Approximations: More Constraint Satisfaction with Fewer Fits. *J. Chem. Phys.* **2005**, *123*, 062201.

(7) Radon, M. Revisiting the Role of Exact Exchange in DFT Spin-State Energetics of Transition Metal Complexes. *Phys. Chem. Chem. Phys.* **2014**, *16*, 14479–14488.

(8) Pinter, B.; Chankisjijev, A.; Geerlings, P.; Harvey, J. N.; De Proft, F. Conceptual Insights into DFT Spin-State Energetics of Octahedral Transition-Metal Complexes through a Density Difference Analysis. *Chem. Eur. J.* **2018**, *24*, 5281–5292.

(9) Weigend, F.; Ahlrichs, R. Balanced Basis Sets of Split Valence, Triple Zeta Valence and Quadruple Zeta Valence Quality for H to Rn: Design and Assessment of Accuracy. *Phys.*

Chem. Chem. Phys. **2005**, *7*, 3297.

(10) Neese, F. The ORCA Program System. *Wiley Interdiscip. Rev. Comput. Mol. Sci.* **2012**, *2*, 73–78.

(11) Neese, F.; Wennmohs, F.; Hansen, A.; Becker, U. Efficient, Approximate and Parallel Hartree–Fock and Hybrid DFT Calculations. A 'Chain-of-Spheres' Algorithm for the Hartree–Fock Exchange. *Chem. Phys.* **2009**, *356*, 98–109.

(12) Eichkorn, K.; Weigend, F.; Treutler, O.; Ahlrichs, R. Auxiliary Basis Sets for Main Row Atoms and Transition Metals and Their Use to Approximate Coulomb Potentials. *Theor. Chem. Accounts Theory, Comput. Model. (Theoretica Chim. Acta)* **1997**, *97*, 119–124.

(13) Grimme, S.; Ehrlich, S.; Goerigk, L. Effect of the Damping Function in Dispersion Corrected Density Functional Theory. *J. Comput. Chem.* **2011**, *32*, 1456–1465.

(14) Grimme, S.; Antony, J.; Ehrlich, S.; Krieg, H. A Consistent and Accurate Ab Initio Parametrization of Density Functional Dispersion Correction (DFT-D) for the 94 Elements H-Pu. *J. Chem. Phys.* **2010**, *132*, 154104.

(15) Kruse, H.; Grimme, S. A Geometrical Correction for the Inter- and Intra-Molecular Basis Set Superposition Error in Hartree-Fock and Density Functional Theory Calculations for Large Systems. *J. Chem. Phys.* **2012**, *136*, 154101.

(16) Bowles, R. S.; Kolstad, J. J.; Calo, J. M.; Andres, R. P. Generation of Molecular Clusters of Controlled Size. *Surf. Sci.* **1981**, *106*, 117–124.

(17) Chao, L. C.; Andres, R. P. Synthesis of a Supported Metal Catalyst Using Nanometer-Size Clusters. *J. Colloid Interface Sci.* **1994**, *165*, 290–295.

(18) Osifchin, R. G.; Mahoney, W. J.; Bielefeld, J. D.; Andres, R. P.; Henderson, J. I.; Kubiak, C. P. Synthesis of a Quantum Dot Superlattice Using Molecularly Linked Metal Clusters.

Superlattices Microstruct. **1995**, *18*, 283–289.

(19) Ayers, T. M.; Fye, J. L.; Li, Q.; Duncan, M. A. Synthesis and Isolation of Titanium Metal Cluster Complexes and Ligand-Coated Nanoparticles with a Laser Vaporization Flowtube Reactor. *J. Clust. Sci.* **2003**, *14*, 97–113.

(20) Ard, S.; Dibble, C. J.; Akin, S. T.; Duncan, M. A. Ligand-Coated Vanadium Oxide Clusters: Capturing Gas-Phase Magic Numbers in Solution. *J. Phys. Chem. C* **2011**, *115*, 6438–6447.

CHAPTER 3

STRUCTURES AND ENERGETICS OF CHROMIUM BENZENE COMPLEXES PREDICTED BY DFT CALCULATIONS

Introduction

Metal-benzene complexes are well known in organometallic chemistry for many years.[1–9] Discoveries of species such as ferrocene and bis(benzene)chromium evoked the concept of the 18-electron rule.[10–12] In 1965, ten years after the discovery of di-benzene chromium and the proposal of its structure, X-ray diffraction experiment confirmed the D_{6h} sandwich structure with benzene rings in an eclipsed configuration.[13] The computations here adopt these known structures as starting geometries.

The properties of mono(benzene)chromium and bis(benzene)chromium have been thoroughly studied in both the condensed phase and gas phase. Electron spin resonance (ESR) spectra of ionic bis(benzene)chromium complexes suggested that the electrons of chromium have strong interactions with the π electrons of benzene.[14,15] A calorimetry study by Conner et al. showed that the dissociation of both benzene from bis(benzene)chromium requires 78 kcal/mol (3.39eV) with a spin cross over from the singlet of bis(benzene)chromium to the septet of ground state Cr.[16] Penner et al. performed photodissociation and photoionization of bis(benzene)chromium and proposed the possible formation of mono(benzene)chromium from the decomposition of $Cr(C_6H_6)_2$.[17] Bond energies of ionized chromium benzene complexes were measured by Armentrout and co-workers,[18] Dunbar and co-workers,[19] and Baer and co-workers[20,21] using different methods. The photoelectron spectra of $Cr(C_6H_6)_2$ were measured by several groups.[22–

[25] Several groups have reported vertical ionization energies of 5.4 – 5.7 eV.[22–29] Richardson and co-workers also measured an adiabatic ionization energy of 5.45 eV through an electron-transfer equilibrium experiment.[25]

Numerous calculations have been reported on these systems as well. The present study uses the chosen DFT methods to calculate the structures, binding energies and ionization energies of mono(benzene)chromium and bis(benzene)chromium. These results are compared with experimental data to validate our calculation methods.

Model Setup

Bis(benzene)chromium has D_{6h} symmetry.[13] Computations here begin with geometries of $Cr(bz)_2$ (bz=benzene) complexes for optimization where the benzenes are in an eclipsed configuration and the chromium is aligned to the centroids of the benzenes. In the geometry optimization of $Cr(bz)_1$ complexes, the structures are initialized with Cr sitting over the centroid of benzene, which has C_{6v} symmetry. The geometry optimizations are relaxed for all atoms without any symmetry restrictions.

Calculations without the RIJCOX approximation are also performed. The results are compared to assess the discrepancies caused by RIJCOX. Similarly, energies without the gCP correction are investigated to check for its effect.

Binding energies are calculated with spin crossover. Cr atom is in its septet spin state (S=6) and Cr^+ has a sextet spin state (S=5). $Cr(bz)_1$ complexes are in high spin states, namely the same multiplicities as those for their corresponding Cr atom or cation. $Cr(bz)_2$ neutral complex is known to have no unpaired electrons. Therefore the spin multiplicities are set to singlet (S=0)

for neutral complexes and doublet (S=1) for cations. Spin states are deliberately selected when calculating ionization potentials. In order to compare the results with experimental data, the septet $Cr(bz)_1$ is ionized to the sextet $Cr(bz)_{1+}$ and the singlet $Cr(bz)_2$ is ionized to the doublet $Cr(bz)_{2+}$.

Structures and Spin Multiplicities

$Cr(bz)_1$ structures have not yet been experimentally determined. Previous theoretical studies suggest that they have C_{6v} symmetry in the high spin states.[19,30] Optimized structures from this work also have symmetries close to C_{6v}, where the Cr aligns to the centroid of the benzene ring. Because no symmetry restriction is applied here, sometimes the carbon atoms move out of the benzene planes after geometry optimizations. For example, the low-spin (M=2) cationic structure shown in Figure 3.1 has one carbon atom apparently located further away from the Cr than the other carbon atoms. This is probably due to the breaking of symmetry caused by the unpaired electrons in higher spin states. From Figure 3.1, we can observe that the distance between the Cr and the benzene ring is much larger in the septet state (M=7) than in other spin states. The general trend is that the Cr-ring distance increases with the spin multiplicity. Specifically in the results from B3LYP calculations, the Cr-ring distance is 1.55 Å in the singlet, 1.69 Å in the doublet, 2.22 Å in the sextet, and 2.88 Å in the septet. Different DFT methods predict different values for the Cr-ring distances. According to a previous X-ray crystallography study, the Cr-ring distance in the singlet $Cr(bz)_2$ is 1.7 Å. The computations here give 1.65, 1.61, and 1.60 Å with B3LYP, PBE, and M06L, respectively. B3LYP out-performs the other two in predicting the Cr-ring distance for the singlet bis(benezene)chromium, while we do not know how these DFT methods perform for the other complexes. These distances may not be reliable because DFT methods are usually not good at predicting non-covalent bond distances.

Nevertheless, the trend of distances varying with multiplicities is consistent through all the methods. This is also true for $Cr(bz)_2$ and $Cr(bz)_2^{2+}$. The Cr-ring distances in the $Cr(bz)_2$ complexes (B3LYP) are 1.65 Å in the singlet and 3.36 Å in the septet for the neutral complexes. They are 1.66 Å in the doublet and 2.34 Å in the sextet for the cationic complexes. These distances are longer than those in the $Cr(bz)_1$ complexes. This indicates that the electrostatic interaction is not the dominant force determining the Cr-benzene distance.

The spin multiplicities predicted in this work are consistent with those reported in previous theoretical and experimental studies. Table 3.1 shows the relative energies of $Cr(bz)_1$ complexes in different spin multiplicities. All three DFT methods predict the ground state to be the highest possible spin state, namely M=7 for neutral $Cr(bz)_1$ and M=6 for cationic $Cr(bz)_1^{1+}$. However, apparently B3LYP predicts a much greater energy difference between the low and high spin states. Specifically, the energy of the singlet $Cr(bz)_1$ predicted by B3LYP is 42.8 kcal/mol relative to that of the septet. The other two methods predict this value less than one third of that predicted by B3LYP. Previous studies have shown that exact HF exchange functionals tend to over stabilize high spin states, which is a characteristic of B3LYP.[31,32] Therefore, the energies of $Cr(bz)_1$ complexes in high spin states (M=6, 7) will be lower with B3LYP than with PBE and M06L, and the low spin states will in turn exhibit relatively higher energies.

As shown in Table 3.2, $Cr(bz)_2$ complexes have low spin states (M=1, 2) as their ground states. However, B3LYP does not find the doublet as the minimum energy spin state of $Cr(bz)_2^{2+}$. If RIJCOX acceleration and gCP correction are not used in the calculations, B3LYP finds the minimum energy for the doublet. Even so, the energy difference (1.1 kcal/mol) between the doublet and the sextet is small compared to the common error of DFT calculations (~2-3 kcal/mol), which means that we cannot be sure about the ground state. This effect is possibly

due to the exact HF exchange functionals in B3LYP, which makes the energies of the high spin states much lower than those predicted by PBE and M06L.

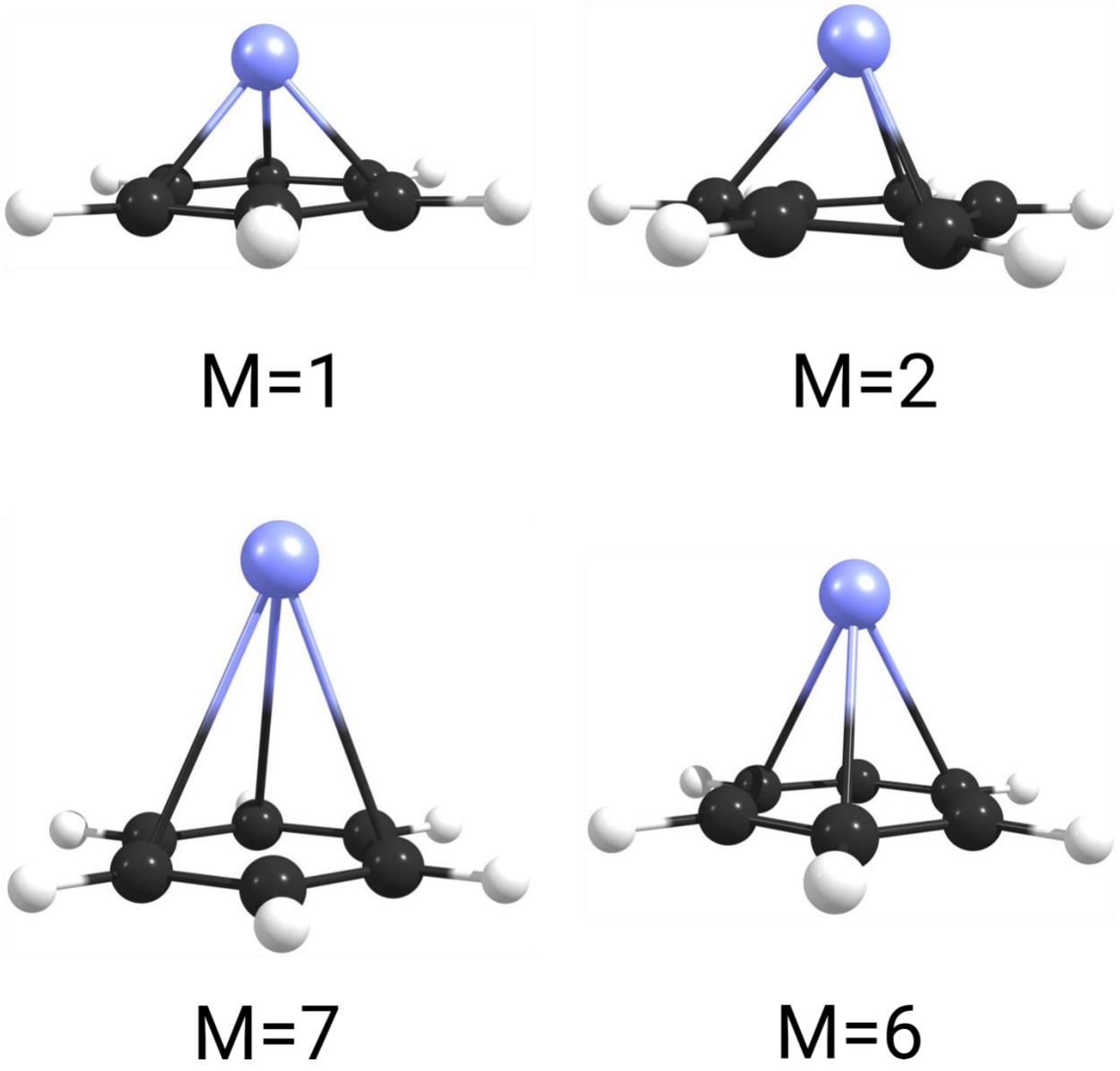

Figure 3.1 Selected optimized $Cr(bz)_1$ structures in neutral (M=1, 7) and cationic (M=2, 6) forms, with their lowest and highest possible spin states.

Table 3.1 Relative total energies (E or E′, in kcal/mol) of $Cr(bz)_1$ neutral and cationic complexes, and the effects of RIJCOX (ΔRI) and gCP (ΔgCP). Prime superscripts (′) indicate that DFT methods include RIJCOX and gCP, i.e. $E'_{DFT} = E_{DFT} + \Delta RI + \Delta gCP$.

Complex	M	E'_{B3LYP}	ΔRI	ΔgCP	E'_{PBE}	ΔRI	ΔgCP	E'_{M06L}	ΔRI	ΔgCP
	1	42.8	-0.4	+7.1	14.1	+0.7	+7.2	11.9	-0.0	+7.4
	3	39.3	-0.2	+6.8	13.0	-0.0	+7.0	12.9	-0.1	+7.0
	5	20.5	-0.1	+6.0	4.8	-0.0	+6.3	0.5	-0.0	+6.3
$Cr(bz)_1$	7	0.0	-0.1	+4.1	0.0	-0.1	+4.5	0.0	+0.2	+4.5
	2	44.3	-0.7	+6.3	26.6	-2.8	+6.7	31.9	-0.1	+7.0
	4	29.8	-0.2	+6.3	16.0	-0.0	+6.5	17.0	-0.1	+6.6
$Cr(bz)_{1+}$	6	0.0	-0.1	+5.1	0.0	-0.0	+5.5	0.0	+0.1	+5.6

Table 3.2 Relative total energies (E or E′, in kcal/mol) of $Cr(bz)_2$ neutral and cationic complexes, and the effects of RIJCOX (ΔRI) and gCP (ΔgCP). Prime superscripts (′) indicate that DFT methods include RIJCOX and gCP, i.e. $E'_{DFT} = E_{DFT} + \Delta RI + \Delta gCP$.

Complex	M	E'_{B3LYP}	ΔRI	ΔgCP	E'_{PBE}	ΔRI	ΔgCP	E'_{M06L}	ΔRI	ΔgCP
	1	0.0	-0.3	+13.6	0.0	-0.0	+13.7	0.0	-0.0	+14.1
	3	23.2	-0.3	+12.6	30.3	+0.3	+12.8	28.0	-0.1	+13.0
	5	23.2	-0.3	+10.4	45.0	+8.4	+11.0	33.8	-0.0	+11.1
$Cr(bz)_2$	7	22.4	-21.2	+9.9	80.3	-0.0	+10.2	58.6	+0.2	+10.4
	2	1.1	-0.3	+13.5	0.0	-0.1	+13.6	0.0	-0.1	+14.0
	4	15.1	-0.4	+11.0	31.4	-0.0	+12.1	21.3	-0.1	+12.2
$Cr(bz)_2^{2+}$	6	0.0	-0.1	+9.7	39.3	-0.1	+10.1	21.2	+0.1	+10.3

The data in Table 3.1 and 3.2 show that the errors introduced by the RIJCOX approximation are small enough to be ignored. Some of the extraordinarily high ΔRI values result because the geometry optimizations with RIJCOX do not converge to a stable minimum. Without the RIJCOX approximation, the self-consistent field (SCF) calculations are not even possible for larger systems such as chromium coronene complexes. Afterall, RIJCOX is a very helpful approximation to greatly accelerate the calculations without introducing much error. Geometric counterpoise (gCP) is a cheap tool to correct the basis set superposition error (BSSE).[33] It is done after each geometry optimization cycle with little cost. The closer two fragments are, the basis sets are going to have more superpositions, thus gCP will add more to the total energy. Given that the structures in high spin states have the Cr and benzene ring further apart, gCP affects the energies in the low spin states more. That is shown in Table 3.1 and 3.2. ΔgCP values are greater in the low spin states where the Cr-ring distances are shorter. Even though gCP will add 10 kcal/mol or more to the exact total energies, ΔgCP values are always positive and the differences between each spin states are not so large. As a result, the application of the gCP correction usually does not change the order of relative energies. In general, gCP is a cheap and useful correction to be used in this study.

Binding Energies

The dissociation of $Cr(bz)_2^{0/+}$ complexes may be composed of two consecutive steps. The first is the loss of benzene:

$$Cr(bz)_2^{0/+} \rightarrow Cr(bz)_1^{0/+} + bz$$

According to the results shown later, the ionization potential of $Cr(bz)_1$ is much lower than the 9.2 eV value of benzene. Therefore, after the dissociation of $Cr(bz)_2^{+}$, the charge should stay on

the metal complex instead of on the benzene. The second step is the loss of the other benzene, which equals the dissociation of $Cr(bz)_1^{0/+}$:

$$Cr(bz)_1^{0/+} \rightarrow Cr^{0/+} + bz$$

The ionization potential of Cr is about 6.77 eV, which is lower than that of benzene. So the cationic $Cr(bz)_1^{+}$ dissociates into a Cr^{+} cation and a neutral benzene.

The calculated binding energies in this work comply with the Wigner-Witmer spin conservation rules.[34] Because the ground state of $Cr(bz)_2$ is a singlet, both of the products in the first step are singlets. Similarly, the doublet $Cr(bz)_2^{2+}$ generates a doublet $Cr(bz)_1^{+}$ and a singlet neutral benzene. Because Cr atom is a septet, the binding energies are calculated for septet $Cr(bz)_1$ and sextet $Cr(bz)_1^{+}$ from septet Cr and sextet Cr^{+}, respectively. If this is the real situation, the spin multiplicities of $Cr(bz)_1$ complexes change between step one and step two. In other words, there is an intersystem crossing (ISC) before $Cr(bz)_1^{0/+}$ further dissociates so that the spin states can cross from septet/sextet to singlet/doublet.

Table 3.3 Binding energies (in kcal/mol) predicted by DFT calculations, and the effects of RIJCOX (ΔRI) and gCP (ΔgCP). Prime superscripts (′) indicate that DFT methods include RIJCOX and gCP.

Reaction	Exp.[21]	B3LYP′	ΔRI	ΔgCP	PBE′	ΔRI	ΔgCP	M06L′	ΔRI	ΔgCP
$Cr(bz)_2^{2+} \rightarrow Cr(bz)_1^{1+} + bz$	57.9	74.4	-3.5	-0.6	95.9	-3.3	-2.7	89.8	-3.3	0.0
$Cr(bz)_1^{1+} \rightarrow Cr^{+} + bz$	39.2	41.8	-1.4	0.0	46.2	-1.9	0.0	47.4	-2.0	-0.1
$Cr(bz)_2 \rightarrow Cr(bz)_1 + bz$	64.1	68.7	-2.8	-0.3	82.5	-3.0	-0.8	75.5	-3.0	0.0
$Cr(bz)_1 \rightarrow Cr + bz$	1.4	6.8	-0.5	0.0	4.2	-0.8	+0.1	6.0	-0.9	-0.2

The results from DFT calculations are shown in Table 3.3. The energies listed below the DFT methods have taken RIJCOX and gCP into account. The results are compared to the values obtained by Baer and co-workers via experiments.[21] As is shown in the table, binding energies from the computations are systematically higher than the experimental results. Among the three DFT methods, B3LYP has the binding energies closest to the experimental data. One abnormal number is the binding energy calculated from the first dissociation step of $Cr(bz)^{2+}$. The value predicted by B3LYP is more than 16 kcal/mol higher than the value obtained by experiment. The other two methods are even worse for this value. If the spin conservation rule is violated, namely the doublet $Cr(bz)^{2+}$ dissociates to the quartet $Cr(bz)^{1+}$ and the singlet benzene, the binding energies will be closer to the experimental result. They are 59.9, 85.3 and 57.9 kcal/mol for the dissociation with the spin state cross over from a doublet to a quartet with B3LYP, PBE and M06L respectively. These values match better with the experiment. This may result from a spin crossover happening during the dissociation. In addition, ΔRI and ΔgCP are usually negative, which make the computational results closer to the experimental values.

Table 3.4 Ionization energies (eV) of chromium benzene complexes calculated for both vertical (IP_v) and adiabatic (IP_a) ionizations. Prime superscripts (′) indicate that DFT methods include RIJCOX and gCP.

Transition		$_{6\leftarrow 7}Cr(bz)_1$	$_{2\leftarrow 1}Cr(bz)_2$
Exp.[29]		5.13	5.43
B3LYP	IP_v	5.82	5.24
	IP_a	5.38	5.25
B3LYP′	IP_v	5.81	5.25
	IP_a	5.43	5.24
PBE	IP_v	5.76	5.42
	IP_a	5.35	5.41
PBE′	IP_v	5.79	5.42
	IP_a	5.45	5.41
M06L	IP_v	5.45	5.30
	IP_a	4.99	5.29
M06L′	IP_v	5.45	5.29
	IP_a	5.04	5.28

Ionization Potentials

The calculated vertical and adiabatic ionization potentials are presented in Table 3.4. The selection rule for the multiplicity change of ΔM=1 is applied here. Considering that the theoretical ground state of $Cr(bz)_1$ is a septet, and the experimentally confirmed ground state of $Cr(bz)_2$ is a singlet, the ionization potentials presented here are either $^{6\leftarrow 7}Cr(bz)_1$ or $^{2\leftarrow 1}Cr(bz)_2$. These calculated values are also compared to the experimental data obtained by Kaya and co-workers.[29] For the ionization of the singlet $Cr(bz)_2$ to the doublet, PBE gives us the best values compared with the experiment. The differences between the vertical and adiabatic potentials are very small for $Cr(bz)_2$, whichever DFT method is chosen, suggesting that its structure does not change much after ionization. The RIJCOX approximation and gCP correction have little effects on these values. On the other hand, none of these DFT methods give ionization potentials close to the experimental result for $Cr(bz)_1$. The best of them, which is obtained with M06L′, is 0.9 eV lower than the 5.13 eV value that was derived from the experiment. According to the experiment, the ionization potential of $Cr(bz)_1$ is lower than that of $Cr(bz)_2$ by about 0.3eV. On the contrary, in this work, except in the case of the adiabatic ionization potentials calculated with PBE and M06L′, all the other ionization potentials of $Cr(bz)_1$ are higher than those of $Cr(bz)_2$. Despite the exact values, the adiabatic ionization potential difference between $Cr(bz)_1$ and $Cr(bz)_2$ is 0.24 eV based on the M06L′ predictions, which is closest to the experiment results. It is shown in Table 4.3 that the vertical ionization potentials of $Cr(bz)_1$ are higher than the adiabatic ionization potentials by 0.3 to 0.4 eV. This is due to the significant structure changes after ionization in the theory. In addition, RIJCOX and gCP introduce more discrepancies (up to 1 eV) to the ionization potentials of $Cr(bz)_1$ than to those of $Cr(bz)_2$. This may hint indirectly

that these DFT methods are not very reliable in the calculating energies and structures of $Cr(bz)_1$ in its high spin states.

Summary

The geometry optimizations of DFT calculations result in correct symmetries, at least for $Cr(bz)_2$ complexes. The Cr-ring distance increases as the spin multiplicity increases. The ground spin states are predicted to be singlet for $Cr(bz)_2$, doublet for $Cr(bz)_2^+$, septet for $Cr(bz)_1$ and sextet for $Cr(bz)_1^+$, which are consistent with previous experiments or theoretical calculations. B3LYP is shown to have higher energies for the low spin states and lower energies for the high spin states compared to the other two DFT methods. This causes difficulties in determining the ground spin state of $Cr(bz)_1^+$. The binding energies obtained from all these DFT calculations are systematically higher than the experiment results. B3LYP has the best performance concerning binding energies. However, all of these methods fail to reproduce the energy of losing one benzene from $Cr(bz)_2^+$. This could be either due to the nature of the DFT methods or because the reaction used for evaluating the binding energy violated the spin conservation rule. Ionization potentials are also calculated here. PBE gives the values closest to the experiment for $Cr(bz)_2$, while none of the DFT methods succeeds for $Cr(bz)_1$. By comparing vertical and adiabatic ionization potentials, it can be seen that during adiabatic ionization, the structures of $Cr(bz)_2$ change little and the structures of $Cr(bz)_1$ change much more. It is also shown that the RIJCOX approximation and the gCP correction usually have little effect on the energetics. On the other hand, RIJCOX can greatly accelerate the SCF calculations, which is necessary when calculating larger systems.

References

(1) Winstein, S.; Lucas, H. J. The Coordination of Silver Ion with Unsaturated Compounds. *J. Am. Chem. Soc.* **1938**, *60*, 836–847.

(2) Mulliken, R. S. Molecular Compounds and Their Spectra. II. *J. Am. Chem. Soc.* **1952**, *74*, 811–824.

(3) Andrews, L. J. Aromatic Molecular Complexes of the Electron Donor-Acceptor Type. *Chem. Rev.* **1954**, *54*, 713–776.

(4) Smith, H. G.; Rundle, R. E. The Silver Perchlorate-Benzene Complex, $C_6H_6 \cdot AgClO_4$, Crystal Structure and Charge Transfer Energy. *J. Am. Chem. Soc.* **1958**, *80*, 5075–5080.

(5) Traynham, J. G.; Olechowski, J. R. Complexation of Cyclic Olefins with Aqueous Silver Ion and with Molecular Iodine. *J. Am. Chem. Soc.* **1959**, *81*, 571–574.

(6) Gut, R.; Rueede, J. The Formation of Silver-Arene Complexes in Liquid Anhydrous Hydrogen Fluoride. *J. Organomet. Chem.* **1977**, *128*, 89–93.

(7) Long, N. J. *Metallocenes: An Introduction to Sandwich Complexes*; Wiley-Blackwell: Malden, MA, 1998.

(8) Crabtree, R. H. *The Organometallic Chemistry of the Transition Metals*, Fourth Edi.; John Wiley & Sons, Inc: Hoboken, New Jersey, 2005.

(9) Astruc, D. *Organometallic Chemistry and Catalysis*; Springer, 2007.

(10) Kealy, T. J.; Pauson, P. L. A New Type of Organo-Iron Compound. *Nature* **1951**, *168*, 1039–1040.

(11) Miller, S. A.; Tebboth, J. A.; Tremaine, J. F. Dicyclopentadienyliron. *J. Chem. Soc.* **1952**, 632–635.

(12) Fischer, E. O.; Hafner, W. Di-Benzol-Chrom. *Zeitschrift für Naturforsch.* **1955**, *10b*, 665–

668.

(13) Weiss, E.; Fischer, E. O. Über Aromatenkomplexe von Metallen. II. Zur Kristallstruktur Und Molekelgestalt Des Di-Benzol-Chrom(0). *Zeitschrift für Anorg. und Allg. Chemie* **1956**, *286*, 142–145.

(14) Feltham, R. D.; Sogo, P.; Calvin, M. Electron Spin Resonance Spectrum of Dibenzene Chromium Cation. *J. Chem. Phys.* **1957**, *26*, 1354–1355.

(15) Elschenbroich, C.; Bilger, E.; Koch, J.; Weber, J. Radical Anion of Bis(η_6-Benzene)Chromium. *J. Am. Chem. Soc.* **1984**, *106*, 4297–4299.

(16) Connor, J. A.; Skinner, H. A.; Virmani, Y. Microcalorimetric Studies. Thermal Decomposition and Iodination of Bis(Benzene)Chromium, Bis(Benzene)-Chromium Iodide, and Some (Arene)Chromium Tricarbonyls. *J. Chem. Soc. Faraday Trans. 1 Phys. Chem. Condens. Phases* **1973**, *69*, 1218–1225.

(17) Penner, A.; Amirav, A.; Tasaki, S.; Bersohn, R. Photodissociation and Photoionization and Their Branching Ratio in Bisbenzene Chromium. *Time-of-Flight Mass Spectrom. with Improv. Resolut. Rev. Sci. Instruments* **1993**, *99*, 176–183.

(18) Meyer, F.; Khan, F. A.; Armentrout, P. B. Thermochemistry of Transition Metal Benzene Complexes: Binding Energies of $M(C_6H_6)_{x+}$ (x = 1, 2) for M = Ti to Cu. *J. Am. Chem. Soc.* **1995**, *117*, 9740–9748.

(19) Lin, C. Y.; Dunbar, R. C. Radiative Association Kinetics and Binding Energies of Chromium Ions with Benzene and Benzene Derivatives. *Organometallics* **1997**, *16*, 2691–2697.

(20) Li, Y.; McGrady, J. E.; Baer, T. Metal-Benzene And Metal-CO Bond Energies in Neutral and Ionic $C_6H_6Cr(CO)_3$ Studied by Threshold Photoelectron-Photoion Coincidence

Spectroscopy and Density Functional Theory. *J. Am. Chem. Soc.* **2002**, *124*, 4487–4494.

(21) Li, Y.; Baer, T. Dissociation Kinetics of Energy-Selected $(C_6H_6)_2Cr^+$ Ions: Benzene-Chromium Neutral and Ionic Bond Energies. *J. Phys. Chem. A* **2002**, *106*, 9820–9826.

(22) Evans, S.; Green, J. C.; Jackson, S. E. He(I) Photoelectron Spectra of Some π-Arene Complexes. *J. Chem. Soc. Faraday Trans. 2 Mol. Chem. Phys.* **1972**, *68*, 249–258.

(23) Guest, M. F.; Hillier, I. H.; Higginson, B. R.; Lloyd, D. R. The Electronic Structure of Transition Metal Complexes Containing Organic Ligands. *Mol. Phys.* **1975**, *29*, 113–128.

(24) Brennan, J. G.; Cooper, G.; Green, J. C.; Kaltsoyannis, N.; MacDonald, M. A.; Payne, M. P.; Redfern, C. M.; Sze, K. H. Electron Localization in the Bis-Arene Complexes $[(\eta\text{-}C_6H_6)_2Cr]$ and $[(\eta\text{-}C_6H_5Me)_2Mo]$: An Investigation by Photoelectron Spectroscopy with Variable Photon Energy. *Chem. Phys.* **1992**, *164*, 271–281.

(25) Ryan, M. F.; Richardson, D. E.; Lichtenberger, D. L.; Gruhn, N. E. Gas-Phase Ionization Energetics, Electron-Transfer Kinetics, and Ion Solvation Thermochemistry of Decamethylmetallocenes, Chromocene, and Cobaltocene. *Organometallics* **1994**, *13*, 1190–1199.

(26) Pignataro, S.; Foffani, A.; Distefano, G. ESCA Study of Some Chromium Complexes: Ionization Energies and Multi-Peak Structure of the Spectra. *Chem. Phys. Lett.* **1973**, *20*, 350–355.

(27) Cabelli, D. E.; Cowley, A. H.; Lagowski, J. J. The Bonding in Some Bis(Arene)Chromium Compounds as Indicated by U.V. Photoelectron Spectroscopy. *Inorganica Chim. Acta* **1982**, *57*, 195–198.

(28) Chizhov, Y. V.; Timoshenko, M. M.; Yur'eva, L. P.; Zaitseva, N. N.; Uralets, I. A.; Kravtsov, D. N.; Asfandiarov, N. L. Electronic Structure of Bis-Arene-Chromium

Complexes. *J. Organomet. Chem.* **1989**, *361*, 79–87.

(29) Kurikawa, T.; Takeda, H.; Hirano, M.; Judai, K.; Arita, T.; Nagao, S.; Nakajima, A.; Kaya, K. Electronic Properties of Organometallic Metal−Benzene Complexes [M_n(Benzene)$_m$ (M = Sc−Cu)]. *Organometallics* **1999**, *18*, 1430–1438.

(30) Bauschlicher, C. W.; Partridge, H.; Langhoff, S. R. Theoretical Study of Transition-Metal Ions Bound to Benzene. *J. Phys. Chem.* **1992**, *96*, 3273–3278.

(31) Radon, M. Revisiting the Role of Exact Exchange in DFT Spin-State Energetics of Transition Metal Complexes. *Phys. Chem. Chem. Phys.* **2014**, *16*, 14479–14488.

(32) Pinter, B.; Chankisjijev, A.; Geerlings, P.; Harvey, J. N.; De Proft, F. Conceptual Insights into DFT Spin-State Energetics of Octahedral Transition-Metal Complexes through a Density Difference Analysis. *Chem. Eur. J.* **2018**, *24*, 5281–5292.

(33) Kruse, H.; Grimme, S. A Geometrical Correction for the Inter- and Intra-Molecular Basis Set Superposition Error in Hartree-Fock and Density Functional Theory Calculations for Large Systems. *J. Chem. Phys.* **2012**, *136*, 154101.

(34) Wigner, E.; Witmer, E. E. Über Die Struktur Der Zweiatomigen Molekelspektren Nach Der Quantenmechanik. *Zeitschrift für Phys.* **1928**, *51*, 859–886.

CHAPTER 4

STRUCTURES AND ENERGETICS OF CHROMIUM NAPHTHALENE COMPLEXES PREDICTED BY DFT CALCULATIONS

Introduction

Naphthalene naturally exists in coal tar and crude oil. It is used in the industries of plastics, resins, fuels, and dyes. We also use it in our daily lives as an insecticide to control moths. It consists of two fused benzene rings, which grants it potential to form complexes with chromium in the same way that benzene does.

Two decades after the original preparation of bis(benzene)chromium, bis(naphthalene)chromium was first prepared using chromium atoms.[1,2] More convenient synthesis from organometallic precursors was reported by Ellis and co-workers in 1997.[3] A later calorimeter study showed its enthalpy of dissociation to be 70 kcal/mol, which is slightly lower than that of the benzene complex.[4] The geometric structure was determined to have C_{2v} symmetry by X-ray crystallography and nuclear magnetic resonance spectroscopy.[5,6] Morand and co-workers studied the electronic structure of bis(naphthalene)chromium both experimentally and theoretically.[7,8] Ligand exchange studies have shown that the binding strength of arenes to Cr follows the order benzene > naphthalene > pyrene.[9,10] This indicated that bis(arene)chromium may prefer smaller arenes. The redox potentials between neutral and +1/+2 charged complexes were measured using cyclic voltammetry.[11] With two benzene rings fused together, the size of naphthalene fits well in the trend from benzene to coronene. This study uses DFT methods to study the structures and energetics of chromium naphthalene complexes.

Model Setup

The two benzene rings in a naphthalene are chemically identical. There are 5 different η_6 and η_2 binding sites on each side of the naphthalene surface, as is shown in Figure 4.1. Geometry optimizations of $Cr(naph)_1$ (naph=naphthalene) start with structures where Cr binds to those sites. The optimized structure may end with Cr directly sitting above one carbon, in a σ-bonded configuration. In this case, the structures are named as their closest η_2-bonded structures. The nomenclature for $Cr(naph)_1$ complexes takes the form of *1b*, where 1 represents the number of naphthalene and *b* tells us which binding sites the Cr sits over. An example of *1b* is shown in Figure 4.1.

When there are two naphthalene molecules facing each other and flanking both sides of Cr, not only can the Cr interact with different binding sites on each naphthalene, but also one of the naphthalenes can rotate about the Cr in parallel with the other one. The structures are named following the pattern of $2ab,\theta_{min.}$ 2 means there are two naphthalene molecules. Cr is over the site *a* of one naphthalene and the site *b* of the other naphthalene. In addition, θ_{min} indicates that the staggering angles of the two naphthalene molecules are minimal or close to 0°, where they can have the greatest π-π interaction. Two examples are shown in Figure 4.1. From this chapter on, all the computation results are from calculations with the RIJCOX approximations and the gCP corrections unless otherwise noted.

The geometry optimizations of the $Cr(naph)_{1}^{0/+}$ complexes started with the five structures from *1a* to *1e* respectively at each spin state. For the $Cr(naph)_{2}^{0/+}$ complexes, the geometry optimizations only started with the Cr at the position *2bb*. The staggering angles are set to 0°,

90°, and 180° at the beginning of the calculations, but are simplified to θ_{min} and θ_{max} in the results.

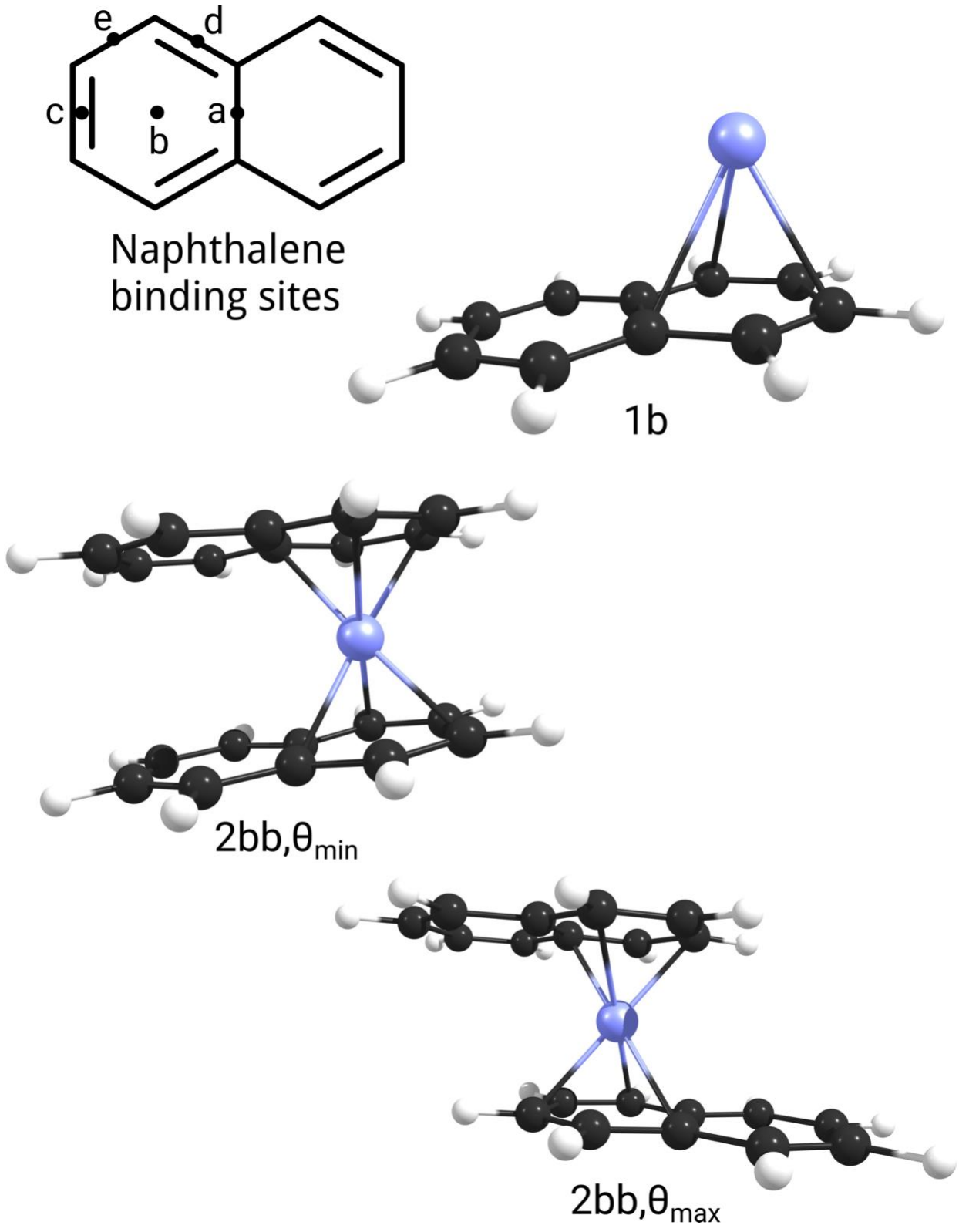

Figure 4.1 Possible binding sites on naphthalene and Cr-naph complex examples.

Geometries and Spin Multiplicities

$Cr(naph)_1$ structures have not yet been experimentally determined. However, it was suggested that the Cr atom prefers to bind to the η_6-type site b in naph-Cr-L complexes, where L stands for other ligands.[5] Table 4.1 and 4.2 show the relative energies of optimized $Cr(naph)_{1+/0}$ structures in different spin states from this study. B3LYP and PBE both predict a septet (M=7) to be the ground spin state for the neutral complexes, while M06L predicts it to be a quintet (M=5). However, the energy differences between the quintet and the septet are very small with PBE and M06L computations. Given the common error of 2-3 kcal/mol for DFT calculations, we cannot determine which of these two truly has the lowest energy. For the cationic complexes $Cr(naph)_{1+}$, on the other hand, all three methods suggest the sextet to be the ground spin state and that is over 10 kcal/mol lower in energy than the quartet.

An interesting aspect of the structures occurs when the Cr binds on naphthalene. Some selected optimized structures are shown in Figure 4.2. *1a*, *1b* and *1d* configurations are predicted to have the minimum energies among neutral complexes with B3LYP, M06L, and PBE calculations, respectively. According to the data shown in Table 4.1, the energy differences between structures in the same spin state with Cr on different binding sites are very small for the neutral complexes. The *1b* configuration is only 0.3 kcal/mol higher in energy than *1a* as septets based on B3LYP calculations. Similarly, the septet structures optimized with M06L (*1b*, *1c*, *1e*) differ in energy by less than 0.1 kcal/mol. The energy difference between the septet *1c* and *1d* is also 0.1 kcal/mol according to PBE. As is seen from these results, the three DFT methods used in this study cannot determine a definitive Cr binding site for the neutral $Cr(naph)_1$. However, their performance is acceptable for the cationic $Cr(naph)_{1+}$ complexes. Most of the geometry optimizations end with Cr^+ binding to the η_6-type site *b*. Even though some of the cation

computations find stable *1a* configurations, their energies are several kcal/mol higher than the those of *1b* configurations. Thus we can conclude that Cr^+ prefers to bind to site *b*, which is over the centroid of the benzene ring.

As we can see from Figure 4.2, the Cr-ring distance varies with the spin multiplicity of the $Cr(naph)_{1}^{0/+}$. Cr atoms or cations farther away from naphthalene planes are in higher spin states (M=6 or 7) rather than in lower spin states (M=1 or 2). To be specific, the Cr-ring distances predicted by M06L in this study are determined to be 1.47, 1.59, 1.61, 1.68, 1.78, 1.98, and 2.37 Å for M=1 to M=7, respectively. These distances predicted by M06L are shorter than those predicted by B3LYP and PBE. B3LYP gives the longest Cr-ring distances among all th ree methods. Even though it is not reasonable to compare these values across DFT methods, the fact that the Cr-ring distance increases as the spin state increases is consistent for each DFT method. If the electrostatic interaction is the dominant force for the Cr-naphthalene bond, we would expect the Cr to be closer to the naphthalene as a cation than as a neutral atom. Given that the Cr-ring distances in cationic complexes are shorter than those in the corresponding neutral complexes (with M-1 spin multiplicities), it is suggested that the electrostatic interaction contributes little to the Cr-naphthalene binding.

Table 4.1 Relative energies (in kcal/mol) of $Cr(naph)_1$ neutral complexes, in different spin states, whose geometries are optimized in theory levels B3LYP, PBE and M06L.

DFT	M	1a	1b	1c	1d	1e
B3LYP	1	-	50.9	-	-	-
	3	50.3	39.0	-	-	-
	5	15.3	14.9	-	14.8	-
	7	**0.0**	0.3	-	-	-
M06L	1	-	24.7	-	-	-
	3	-	20.4	-	-	-
	5	-	**0.0**	-	-	-
	7	-	3.4	3.3	-	3.4
PBE	1	-	21.1	-	-	-
	3	-	17.6	-	31.4	-
	5	-	2.6	-	1.6	10.7
	7	-	-	0.1	**0.0**	-

Table 4.2 Relative energies (in kcal/mol) of $Cr(naph)_{1+}$ cationic complexes, in different spin states, whose geometries are optimized in theory levels B3LYP, PBE and M06L.

DFT	M	1a	1b	1c	1d	1e
B3LYP	2	-	43.2	-	-	-
	4	-	26.0	-	36.9	-
	6	2.5	**0.0**	-	-	-
M06L	2	-	32.8	-	-	-
	4	-	13.1	-	-	-
	6	-	**0.0**	-	-	-
PBE	2	-	26.8	-	-	-
	4	-	11.7	-	-	-
	6	5.0	**0.0**	-	-	-

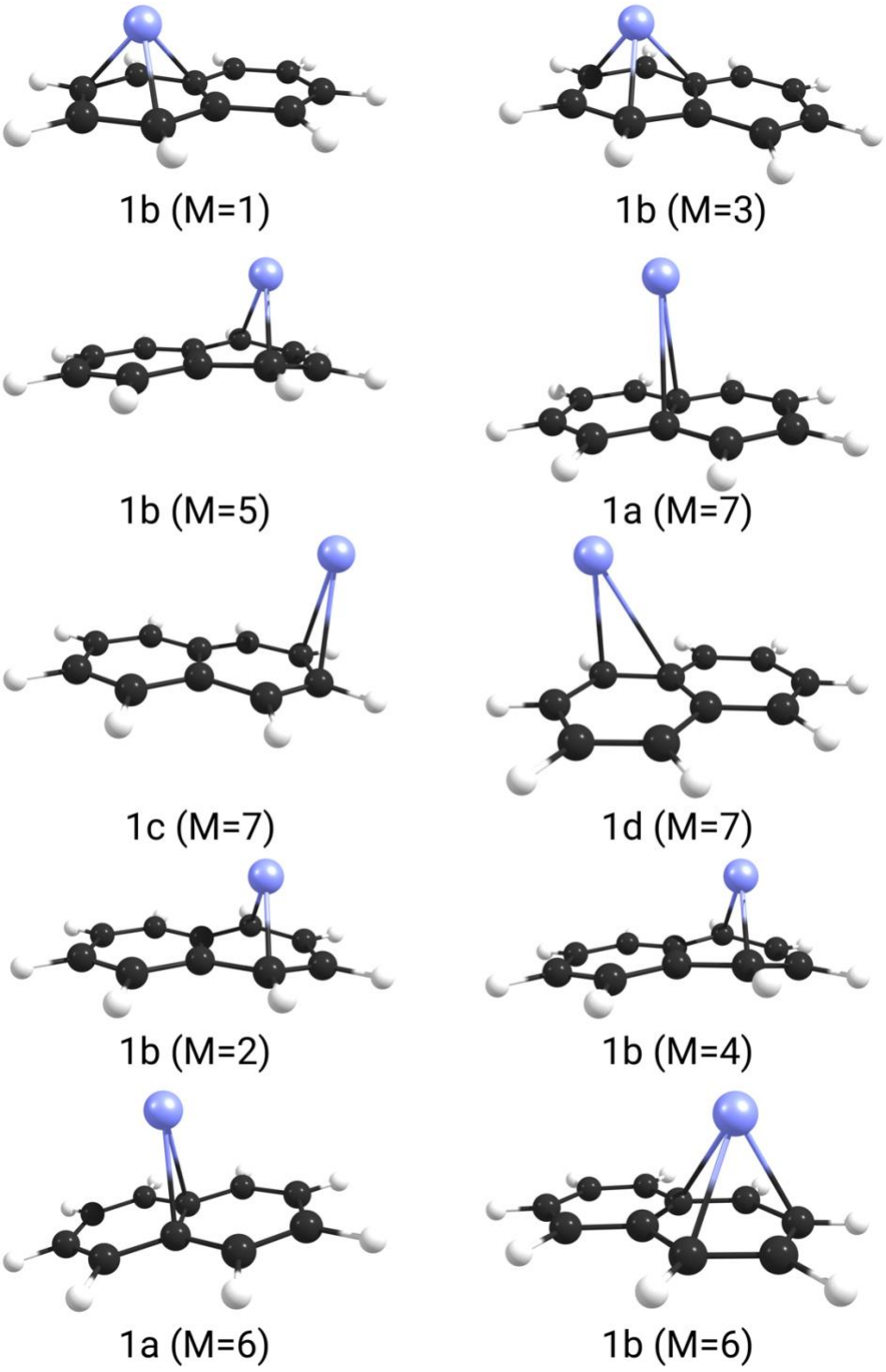

Figure 4.2 Selected $Cr(naph)_1$ structures after geometry optimizations, in neutral (M=1,3,5,7) and cationic (M=2,4,6) forms.

Some of the $Cr(naph)_2^{0/+}$ geometries optimized by DFT methods are shown in Figures 4.3 and 4.4. As in the case of $Cr(naph)_1$, the Cr-ring distances also increase with the spin multiplicities. As a result, $Cr(naph)_2$ complexes should have the same type of bond between Cr and naphthalene as $Cr(naph)_1$ complexes have. The Cr-ring distance in the singlet $Cr(naph)_2$ is about 1.66 Å, as measured in a previous X-ray crystallography study.[6] This distance is calculated to be 1.64, 1.64, and 1.66 Å by PBE, M06L, and B3LYP, respectively. Among the three, B3LYP gives the result that is the closest to that from the crystallography. For both singlet $Cr(bz)_2$ and $Cr(npah)_2$, B3LYP out-performs the other two methods in predicting the Cr-ring distances. Therefore, B3LYP may be the best method to predict Cr-ring distances in Cr-π complexes. There is no experiment data for the complexes in their higher spin states. Thus we cannot be sure whether B3LYP can give the Cr-ring distances closer to the reality than the other two for these systems.

Tables 4.3 and 4.4 present the calculated relative energies of the neutral and the cationic $Cr(naph)_2$ complexes. All three DFT methods predict that the ground spin state of the neutral $Cr(naph)_2$ is a singlet, which is consistent with the experiment. The energy differences between the singlet and the septet calculated by PBE and M06L are relatively large (about 25 kcal/mol). On the other hand, the energy differences between different spin states are small in the B3LYP computations. The energy difference between the singlet and the septet predicted by B3LYP is 7.7 kcal/mol. In addition, B3LYP predicts the sextet to be the ground spin state for the $Cr(naph)_2^{2+}$, while PBE and M06L predict the doublet. This discrepancy between B3LYP and the other two methods is also seen for $Cr(bz)_2^{2+}$, which is attributed to the HF exchange included in the functional.[12,13]

When comparing the energies in the same spin state, but with large and small staggering angles (θ_{min} and θ_{max}) in the structures, we can see that the energy differences are usually less than 4

kcal/mol, except in the B3LYP-calculated low spin states (M=1, 2). Generally, the structures with small staggering angles (θ_{min}), have lower energies, especially in the ground spin states. With small staggering angles, the two conjugated π systems of two naphthalene molecules can overlap more. Therefore the fact that structures with θ_{min} are stable indicate that the π-π interaction plays an important role in stabilizing complexes with two naphthalene molecules. However, the small energy differences between structures with θ_{min} and θ_{max} suggest that the effect of the π-π interaction is not as great as the spin multiplicity on the stability of Cr-naphthalene complexes. The influence of the π-π interaction can be seen from the structures shown in Figures 4.3 and 4.4. It has already been shown that the Cr-naphthalene distance is longer in higher spin states. Hence, it is apparent from the figures that the insertion of a high spin (M>3) Cr pushes two naphthalene molecules away from each other at the Cr-bound ends, while on the other ends the π-π interaction bring them closer together. Hence the naphthalenes in those structures are not parallel, but are tilted like a clamp with the wide end grasping a Cr atom.

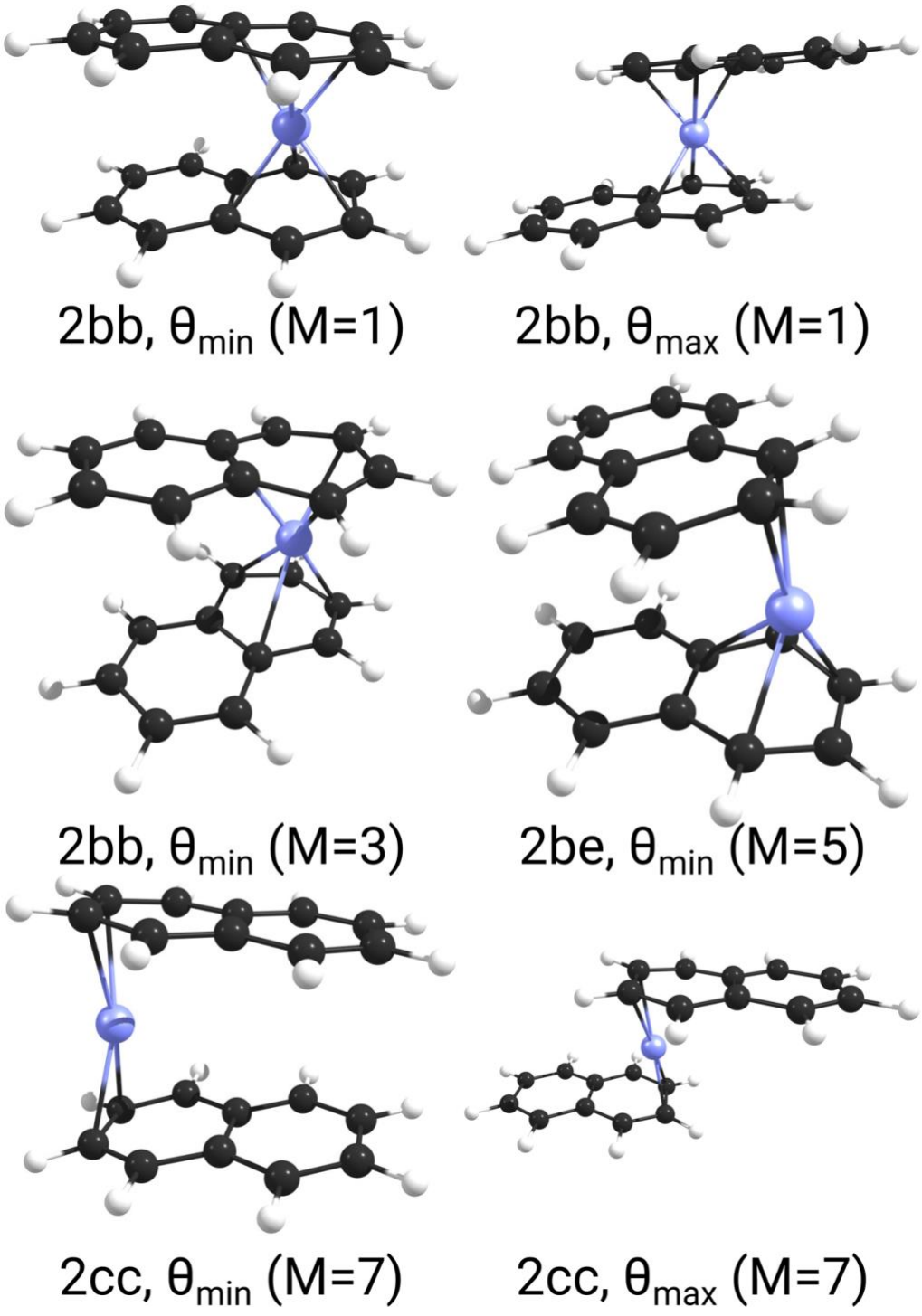

Figure 4.3 Selected structures determined for neutral $Cr(naph)_2$.

Table 4.3 Relative Energies (kcal/mol) relative to the minimum, of $Cr(naph)_2$ complexes with geometries optimized in different theory levels. θ_{min} (or θ_{max}) indicates that two coronene molecules have small (or large) staggering angles.

DFT	M	2bb,θ_{min}	2be,θ_{min}	2cc,θ_{min}	2ee,θ_{min}	2bb,θ_{max}	2cc,θ_{max}	2ee,θ_{max}
B3LYP	1	**0.0**	-	-	-	27.7	-	-
	3	-	6.3[a]	-	-	-	-	6.2
	5	-	-	-	4.0[b]	-	-	2.6[c]
	7	-	-	-	7.7	-	10.7	-
PBE	1	**0.0**	-	-	-	2.4	-	-
	3	8.1	-	-	-	8.2	-	-
	5	-	23.0	-	21.7	-	-	22.7
	7	-	-	38.1	-	25.7	-	40.0
M06-L	1	**0.0**	-	-	-	2.5	-	-
	3	4.1	-	-	-	4.6	-	-
	5	-	14.5	-	-	-	-	12.3[c]
	7	-	-	23.9	-	-	25.8	-

[a] 2bc,θ_{min}

[b] 2de,θ_{min}

[c] 2ce,θ_{min}

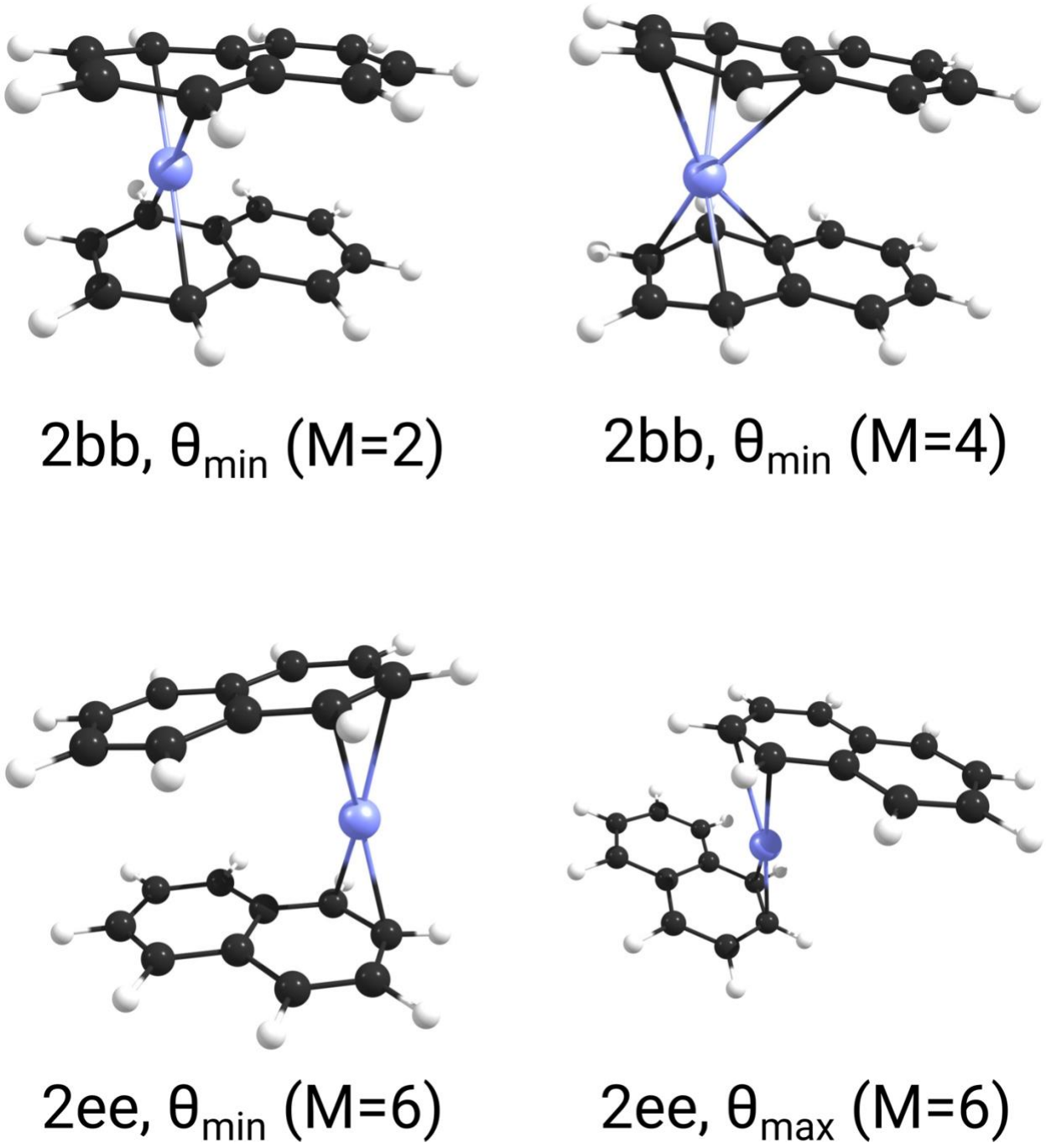

Figure 4.4 Selected structures determined for $Cr(naph)_2^{2+}$.

Table 4.4 Relative Energies (kcal/mol) relative to the minimum, of $Cr(naph)_2^{2+}$ complexes with geometries optimized in different theory levels. θ_{min} (or θ_{max}) indicates that two coronene molecules have small (or large) staggering angles.

DFT		2bb,θ_{min}	2cc,θ_{min}	2ee,θ_{min}	2bb,θ_{max}	2ee,θ_{max}
B3LYP	M=2	17.2	-	-	26.9	-
	M=4	12.1	-	-	11.0	-
	M=6	-	-	**0.0**	-	1.5[a]
PBE	M=2	**0.0**	-	-	1.7	-
	M=4	10.0	-	-	10.2	-
	M=6	-	-	19.1	-	21.6
M06-L	M=2	**0.0**	-	-	1.9	-
	M=4	1.4	-	-	1.4	-
	M=6	-	4.8	-	-	5.8

[a] 2ce,θ_{max}

Binding Energies

The dissociation of $Cr(naph)_2^{0/+}$ complexes may be composed of two consecutive steps. The first is the loss of naphthalene:

$$Cr(naph)_2^{0/+} \rightarrow Cr(naph)_1^{0/+} + naph$$

According to the results shown later, the ionization potential of $Cr(naph)_1$ is much lower than the 8.14 eV value of naphthalene. Therefore, after the dissociation of $Cr(naph)_2^{2+}$, the charge should stay on the metal complex instead of on the naphthalene. The second step is the loss of the other naphthalene, which equals the dissociation of $Cr(naph)_1^{0/+}$:

$$Cr(naph)_1^{0/+} \rightarrow Cr^{0/+} + naph$$

The ionization potential of Cr is about 6.77 eV, which is lower than that of naphthalene. So the cationic $Cr(naph)_1^{1+}$ dissociates into a Cr^+ cation and a neutral naphthalene.

Calculated binding energies of Cr binding to naphthalene molecules are shown in Table 4.5, including binding to the first, the second, and both naphthalene molecules, which are represented by B.E.1, B.E.2, and B.E.sum, respectively. Both the results with the Wigner-Witmer spin conservation rules (M=M´),[14] and with the spin cross over (M≠M´) are shown in Table 4.5. M is the spin multiplicity of the Cr complex with more naphthalene ligands, namely the spin multiplicity of a bare Cr for B.E.1 and B.E.sum, and the spin multiplicity of the $Cr(naph)_1^{0/+}$ for B.E.2. When the spin cross over is taken into account, the spin multiplicity of the Cr complex with fewer naphthalene ligands (M´) is set to its ground spin state predicted by computations. In most cases, M´=7 is chosen for the Cr atom and $Cr(naph)_1$, and M´=6 for Cr^+ and $Cr(naph)_1^{1+}$. An exception is the results of B.E.2 with M06L, since M06L, unlike the other two methods,

predicts the ground spin state of the $Cr(naph)_1$ as a quintet, as seen in Table 4.1. The B.E.1 values for neutral complexes are either negative or very small if we take the spin cross over into consideration. The flip of the electron spins, which happens during the spin cross over, costs energy, thus the binding energies with the spin conservation (M=M´) are always larger than those with the spin cross over (M≠M´), as seen in Table 4.5. Because the energy released from adding the first naphthalene to a Cr is sometimes less than the energy required to flip an electron spin, negative values can be seen in this Table.

The binding energies computed for the naphthalene complexes are compared to those computed for the corresponding benzene complexes in Table 3.3. The binding energies B.E.1 with M = M´= 6 or 7, and B.E.2 with M = M´= 1 or 2 are selected to be compared with those of the benzene complexes. All three DFT methods agree that the B.E.2 of the naphthalene complexes are smaller than those of the benzene complexes. This is also supported by ligand-exchange experiments, which indicate benzene binds stronger to Cr than naphthalene.[9,10] In these experiments, the complexes had two or more ligands on Cr, and the ligand-exchange reactions only substituted one of the ligands. Hence it is reasonable to compare the experiments with the computed B.E.2, but not with the B.E.1. The B.E.1 values computed for the Cr-naphthalene complexes are larger than those computed for the Cr-benzene complexes with B3LYP and PBE. They are larger by about 4 kcal/mol for the cationic complexes, and by about 1.5 kcal/mol for the neutral complexes. However, M06L predicts the B.E.1 for the naphthalene complexes to be smaller than those for the benzene complexes, by 3 and 1 kcal/mol for the neutral and cationic complexes. Unfortunately, no experimental data is available, so that we cannot be sure whether benzene or naphthalene binds stronger to Cr.

Table 4.5 Bond energies (kcal/mol) of Cr binding to the first (B.E.1), the second (B.E.2), and both (B.E.sum) napthalenes, with (M≠M') and without (M=M') spin cross over. B.E.x = $E[Cr(naph)_{x-1}^{0/+}] + E[naph] - E[Cr(naph)_{x}^{0/+}]$. B.E.sum = $E[Cr^{0/+}] + 2E[naph] - E[Cr(naph)_{2}^{0/+}]$.

		B.E.1		B.E.2		B.E.sum	
	M´	M=M´	M≠M´	M=M´	M≠M´	M=M´	M≠M´
B3LYP	1	64.6	-40.4	64.2	15.6	128.8	23.7
	3	19.7	-30.8	48.2	9.3	67.9	17.4
	5	11.2	-6.8	26.6	11.7	37.7	19.8
	7	8.1	-	7.9	-	16.0	-
	2	57.2	2.1	61.3	18.1	118.5	63.4
	4	58.6	19.3	51.3	25.4	109.9	70.7
	6	45.3	-	37.5	-	82.8	-
PBE	1	54.2	-15.1	76.9	55.9	131.1	61.8
	3	45.9	-11.7	65.4	47.8	111.3	53.7
	5	31.2	3.4	36.7	34.2	67.9	40.1
	7	5.9	-	17.8	-	23.6	-
	2	81.9	23.2	86.2	59.4	168.1	109.4
	4	79.0	38.3	61.1	49.4	140.1	99.4
	6	50.5	-	40.3	-	90.2	-
M06L	1	93.1	-18.1	72.9	48.4	166.0	54.8
	3	36.8	-14.0	64.1	43.8	101.0	50.1
	5	20.0	6.4	33.6	-	53.7	40.0
	7	3.1	-	27.7	24.4	30.8	-
	2	75.5	14.1	81.2	48.4	156.7	95.3
	4	75.2	33.8	60.4	47.2	135.6	94.2
	6	46.9	-	44.1	-	91.0	-

Ionization Potentials

The calculated vertical and adiabatic ionization potentials (IP_v and IP_a) are presented in Table 4.6. The selection rule for the multiplicity change of $\Delta M=1$ is applied here. For vertical ionization, the structures of cations are inherited from the neutral clusters. Since the lowest energy computed by M06L for the neutral $Cr(naph)_1$ is a quintet, the IP_a is evaluated as the $M=6\leftarrow5$ transition. In the same manner, the IP_a of $Cr(naph)_2$ computed by B3LYP is evaluated as the $M=6\leftarrow1$ transition. The IP_v values are compared to the IP_v values of benzene complexes shown in Table 3.4. The ionization potentials of ${}_{6\leftarrow7}Cr(naph)_1$ and ${}_{2\leftarrow1}Cr(naph)_2$ are smaller than those of the corresponding ionization of the Cr-benzene complexes. This is probably because naphthalene has a larger conjugated π system to stabilize the cations of the Cr naphthalene complexes.

The ionization potential of $Cr(naph)_2$ is measured to be 5.9 eV using the electron ionization experiment.[15] From Table 4.6, we can see that the IP_v values of $Cr(naph)_2$ from a singlet to a doublet are smaller than the experiment for all three methods The IP_a computed from PBE calculations is 6.03 eV, which is the closest value to the experiment. In both cases of vertical and adiabatic ionizations, PBE gives the ionization potentials that match the experimental result the best. As is discussed in Chapter 3, PBE also predicts the ionization potential of $Cr(bz)_2$ that matches the experiment. From these two instances, we may conclude that PBE is the probably the best DFT method among the three in computing the ionization potentials of the $Cr(PAH)_2$ complexes.

Table 4.6 Vertical ionization potentials (IP_v) and adiabatic ionization potentials (IP_a) of $Cr(naph)_x$ complexes in the unit of eV, where the spin multiplicity change is limited to $\Delta M=\pm 1$ in vertical ionizations. M is the spin multiplicity of a neutral complex, and M´ is the spin multiplicity of a cationic complex.

			PBE		B3LYP		M06L	
Complex	M	M´	IP_v	IP_a	IP_v	IP_a	IP_v	IP_a
	1	2	5.78		4.84		5.67	
	3	2	5.90		5.83		5.68	
x=1	3	4	5.35		4.87		4.91	
	5	4	5.84		6.01		5.78	
	5	6	5.74		5.19		5.52	5.08
	7	6	5.69	5.35	5.69	5.33	5.17	
	1	2	5.23	6.03	5.07	4.38[a]	5.10	5.27
	3	2	5.14		5.81		5.17	
x=2	3	4	5.67		5.05		5.33	
	5	4	5.34		5.45		5.36	
	5	6	5.50		4.42		4.97	
	7	6	4.47		4.16		4.33	

[a] M=1 and M´=6.

Summary

The ground spin states of $Cr(naph)_1$ and $Cr(naph)_2$ are believed to be septet and singlet, and those of their corresponding cations are believed to be sextet and doublet, except that M06L predicts the $Cr(naph)_1$ to be a quintet and B3LYP predicts the $Cr(naph)_{2+}$ to be a sextet. The Cr prefers to bind over the centroid of one benzene ring with a slightly higher binding energy compared to the other sites. The Cr-ring distance increases as the spin multiplicity increases. In the complexes with two naphthalene molecules, the π-π interaction plays an important role in promoting the stability of the complexes. Even though the insertion of a Cr tends to push two naphthalene molecules away, the π-π interaction pulls them together at the ends without the Cr. Therefore one of the naphthalene molecules tilts towards the other naphthalene to form a clamp-like structure, especially in higher spin states. The binding energies of naphthalene to Cr are lower than those of the $Cr(bz)_{2}^{0/+}$ complexes, which is consistent with the previous experiment. The ionization potentials are lower than those of their corresponding benzene complexes, indicating that the larger conjugated π systems contribute to the stability of the cations. According to the results shown in Chapter 3 and Chapter 4, B3LYP is probably the best method among the three to predict the Cr-PAH distances, and the PBE is probably the best method among the three to predict ionization potentials.

References

(1) Elschenbroich, C.; Möckel, R. Bis(η6-naphthalene)Chromium(0). *Angew. Chemie Int. Ed.* **1977**, *16*, 870–871.

(2) Kündig, E. P.; Timms, P. L. Metal Atom Preparation and Ligand Displacement Reactions of Bisnaphthalenechromium and Related Compounds. *J. Chem. Soc., Chem. Commun.* **1977**, 912–913.

(3) Pomije, M. K.; Kurth, C. J.; Ellis, J. E.; Barybin, M. V. First Conventional Syntheses and Isolation of Bis(Naphthalene)Metal(0) Complexes. Structural Characterization of V(η6-$C_{10}H_8$)2. *Organometallics* **1997**, *16*, 3582–3587.

(4) Connor, J. A.; Martinho-Simoes, J. A.; Skinner, H. A.; Zafarani-Moattar, M. T. Thermochemistry of Bis-Arene- and Arenetricarbonyl-Chromium Compounds Containing Hexamethylbenzene, 1,3,5-Trimethylbenzene and Naphthalene. *J. Organomet. Chem.* **1979**, *179*, 331–356.

(5) Desobry, V.; Kündig, E. P. A 13C-NMR. Study of Naphthalene Chromium Complexes. Correlation with Reactivity: Nucleophilic Aromatic Substitution Reactions. *Helv. Chim. Acta* **1981**, *64*, 1288–1297.

(6) Elschenbroich, C.; Möckel, R.; Massa, W.; Birkhahn, M.; Zenneck, U. Bis(H6-naphthalin)Chrom(0): Röntgenstrukturbestimmung Und Kernresonanzspektroskopische Untersuchung. *Chem. Ber.* **1982**, *115*, 334–345.

(7) Morand, P. D.; Francis, C. G. Modeling Macroscale Metal Vapor Reactions: Synthesis of Bis(η6-Naphthalene)Titanium. *Inorg. Chem.* **1985**, *24*, 56–61.

(8) Osborne, J. H.; Trogler, W. C.; Morand, P. D.; Francis, C. G. Electronic Structures of Bis(Benzene)Chromium and the C_{2h} and C_{2v} Isomers of Bis(Naphthalene)Chromium.

Organometallics **1987**, *6*, 94–100.

(9) Bush, B. F.; Lynch, V. M.; Lagowski, J. J. Transition-Metal Organometallic Compounds: 8: Arene Exchange Reactions of Bis(Naphthalene)Chromium. *Organometallics* **1987**, *6*, 1267–1275.

(10) Howell, J. A. S.; Ashford, N. F.; Dixon, D. T.; Kola, J. C.; Albright, T. A.; Kang, S. K. The Arene-Exchange Reaction in Naphthalene- and Pyrene-$Cr(CO)_3$. *Organometallics* **1991**, *10*, 1852–1864.

(11) Bush, B. F.; Lagowski, J. J. The Electrochemical Properties of the (μ-η_6,η_6-Naphthalene)Dichromium Compounds and Bis(η_6-Naphthalene)Chromium. *J. Organomet. Chem.* **1990**, *386*, 37–50.

(12) Radon, M. Revisiting the Role of Exact Exchange in DFT Spin-State Energetics of Transition Metal Complexes. *Phys. Chem. Chem. Phys.* **2014**, *16*, 14479–14488.

(13) Pinter, B.; Chankisjijev, A.; Geerlings, P.; Harvey, J. N.; De Proft, F. Conceptual Insights into DFT Spin-State Energetics of Octahedral Transition-Metal Complexes through a Density Difference Analysis. *Chem. Eur. J.* **2018**, *24*, 5281–5292.

(14) Wigner, E.; Witmer, E. E. Über Die Struktur Der Zweiatomigen Molekelspektren Nach Der Quantenmechanik. *Zeitschrift für Phys.* **1928**, *51*, 859–886.

(15) Herberich, G. E.; Müller, J. Massenspektren Und Stabilitäten von Diaromatenchromkomplexen. *J. Organomet. Chem.* **1969**, *16*, 111–117.

CHAPTER 5

STRUCTURES AND ENERGETICS OF CHROMIUM PYRENE COMPLEXES PREDICTED BY DFT CALCULATIONS

Introduction

Like naphthalene, pyrene naturally exists in coal tar, but in lower amounts. It consists of four fused benzene rings. We can also imagine it as a coronene but with three peripheral rings removed. Therefore, its size makes it a good candidate for us to study the trend from benzene to coronene.

So far, there are only a few published papers studying chromium pyrene complexes, including some about Cr complexes of pyrene and tricarbonylchromium.[1,2] It has been shown that one pyrene molecule can support more than one metal atom on both sides and on different benzene rings.[1] On the other hand, loading chromium atoms on both sides of a benzene to form an elongated multi-decker complexes is very difficult.[3] A ligand exchange study has shown that pyrene binds to chromium weaker than naphthalene.[4] The weak interaction with Cr is probably why bis(pyrene)chromium has not yet been successfully synthesized. Nevertheless, many studies have been performed on pyrene complexes with other metal atoms or ions.[5–9]

Pyrene has two sets of six-member rings that are chemically identical, namely the α rings and the β rings. An α ring shares three carbon atoms with the adjacent rings and a β ring shares four carbon atoms. The point group of a pyrene is D_{2h}, which is a lower symmetry than the D_{6h} of a coronene. As a result, there are more possible binding sites on pyrene than on coronene. Here in

this study, several DFT methods are used to study the structures and energetics of Cr-pyrene complexes.

Model Setup

Given the symmetry, There are eight chemically different η_6 and η_2 binding sites on each side of a pyrene, as shown in Figure 5.1. Geometry optimizations of $Cr(pyr)_1$ (pyr=pyrene) start with structures where Cr binds to those sites. An optimized structure may have the Cr sitting directly above one carbon, in a σ-bonded configuration. In these cases, structures are named as their closest η_2-bonded structures. The nomenclature for the $Cr(pyr)_1$ complexes takes the form of *1f*, where 1 represents the number of pyrene molecules and *f* indicates that Cr sits over the centroid of the α ring. Examples of *1c* and *1f* structures are shown in Figure 5.1.

When there are two pyrene molecules facing each other and flanking Cr on opposite positions, The structures can vary not only with different Cr-binding sites on each pyrene, but also with the angle of one pyrene rotating about the Cr parallel to the other one. The structures are named following the pattern *2ag*,$\theta_{max.}$ 2 indicates that there are two pyrene molecules. Cr is over the site *a* of one pyrene and the site *g* of the other pyrene. In addition, θ_{max} indicates that the staggering angle of the two pyrene molecules is maximized or close to 180°, where they have the least π-π interaction. Two examples are shown in Figure 5.1.

The geometry optimizations of the $Cr(pyr)_{1}^{0/+}$ complexes start with the eight structures from *1a* to *1h* respectively at each spin state. For the $Cr(pyr)_{2}^{0/+}$ complexes, the geometry optimizations start with the Cr at the positions *2bb*, *2ff*, and *2bf*. The staggering angles are set to 0°, 90°, and 180° at the beginning of the calculations, but these are simplified to θ_{min} and θ_{max} in the results.

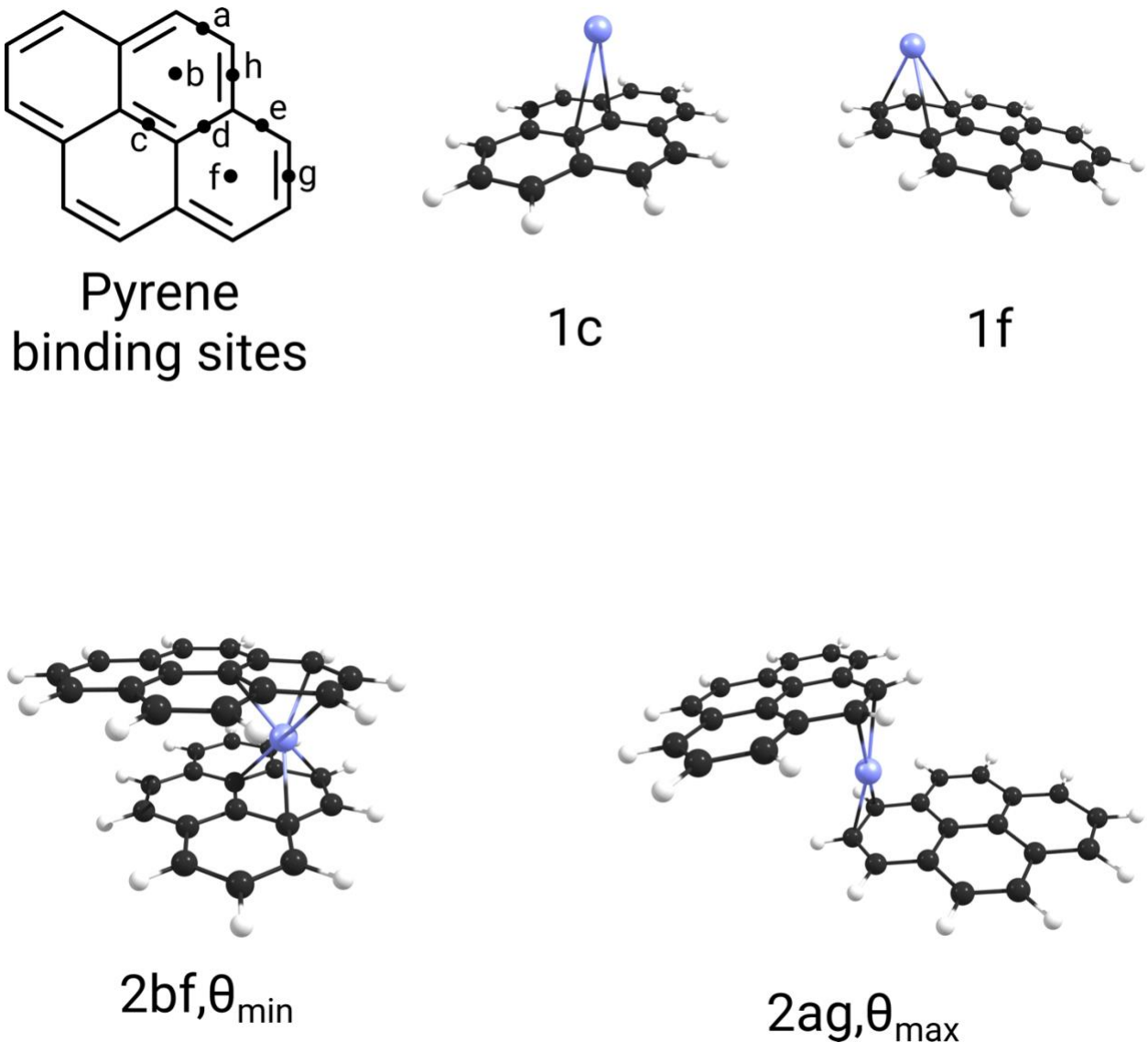

Figure 5.1 Possible binding sites on pyrene and Cr-pyrene complexes.

Geometries and Spin Multiplicities

No experiments are available which have determined the structures of $Cr(pyr)_1$ or $Cr(pyr)_2$. Structures of pyrene-tricarbonylchromium complexes have indicated that the α ring of a pyrene is likely the preferable binding site for Cr.[1,2] Tables 5.1 and 5.2 present the computed relative energies of the $Cr(pyr)_{1^{0/+}}$ complexes with the Cr binding to different positions on the pyrene, and with different electron spin multiplicities. For different structures with the same spin multiplicities, the energy differences between the complexes with the Cr binding to the α and the β ring (< 3 kcal/mol) are small in the high spin states (M = 5, 6, or7). In the low spin states (M = 1, 2, 3, or 4), the energy differences between *1a*/*1b* and *1f*/*1g* are as large as 3-10 kcal/mol, suggesting that the Cr prefers to bind to the β ring. However, as predicted by the calculations, the ground spin state of the $Cr(pyr)_1$ is a quintet or a septet. Therefore, it not clear where the Cr prefers to bind on the pyrene based only on the computational results.

M06L predicts that the ground state of the $Cr(pyr)_1$ is a quintet instead of a septet as predicted by B3LYP and PBE. Nevertheless, the septet *1g* is only 0.4 kcal/mol higher energy than the ground state in the M06L computational results. This difference is too small to determine which is the true ground state. If results from all three methods are taken into consideration, it is very possible that the septet (M =7) is the ground spin state of the $Cr(pyr)_1$, as in the case of the $Cr(bz)_1$ and the $Cr(naph)_1$. The three DFT methods agree with each other that the ground state spin of $Cr(pyr)_{1^+}$ is a sextet (M = 6), consistent with the sextet found for the one-ligand Cr complexes of benzene and naphthalene.

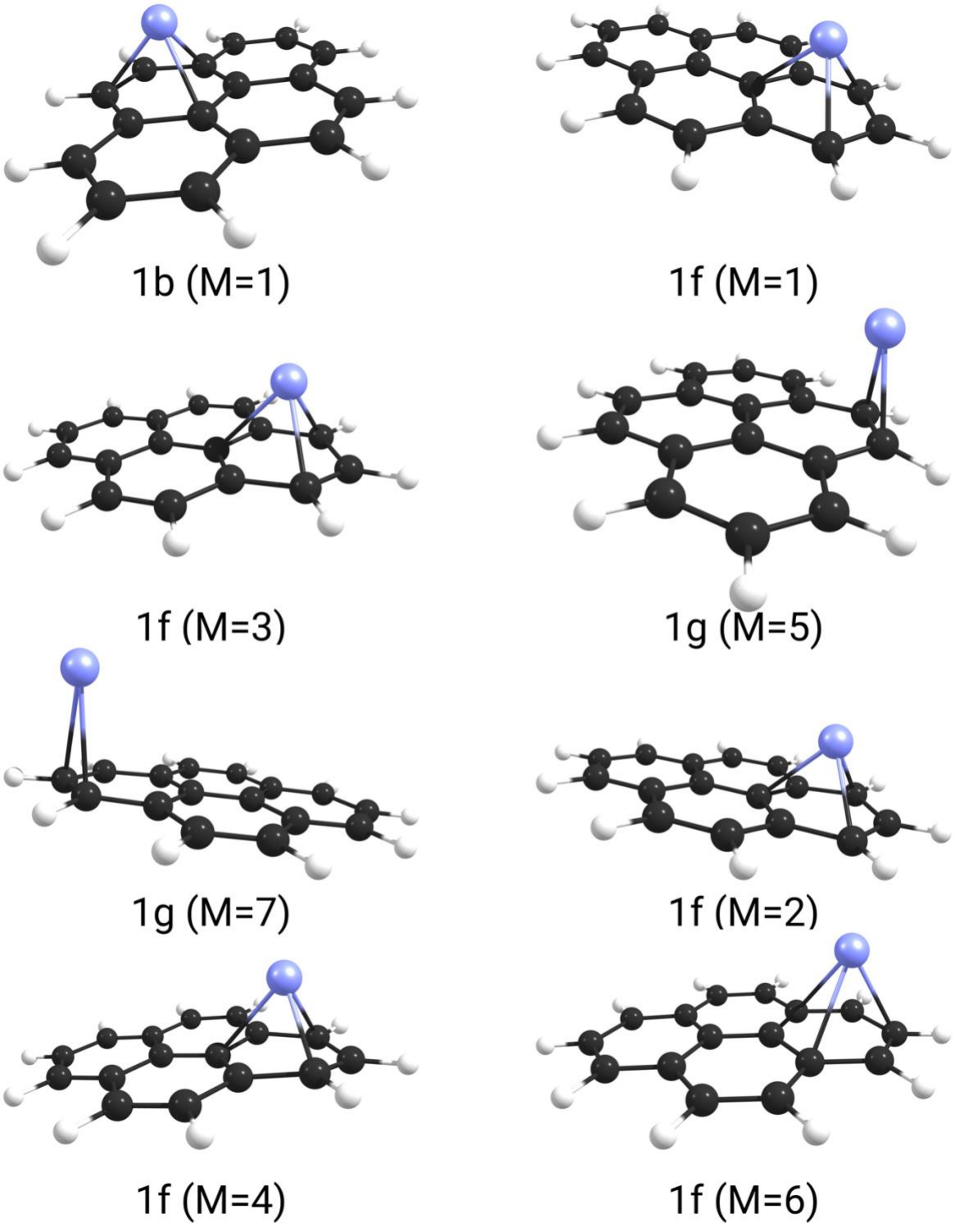

Figure 5.2 Selected $Cr(naph)_1$ structures in neutral (M=1,3,5,7) and cationic (M=2,4,6) forms.

Table 5.1 Relative energies (in kcal/mol) of $Cr(pyr)_1$ neutral complexes, in different spin states, whose geometries are optimized in theory levels B3LYP, PBE and M06L.

DFT	M	1a	1b	1c	1d	1e	1f	1g	1h
B3LYP	1	-	64.9	101.8	-	64.9	53.0	96.7	-
	3	39.4	-	51.3		42.4	44.1	44.0	-
	5	14.0	-	15.7	15.9	15.1	-	15.1	-
	7	-	-	**0.0**	0.4	0.9	1.2	-	0.7
PBE	1	40.6	33.9	-	-	-	23.4	-	33.9
	3	30.5	27.3	-	-	-	19.7	-	-
	5	3.9	-	25.3	-	-	6.4	-	-
	7	1.2	-	2.6	-	-	-	**0.0**	-
M06L	1	-	37.7	87.7	-	-	24.5	-	-
	3	29.5	28.4	-	-	34.6	18.9	-	29.9
	5	**0.0**	-	13.4	-	3.6	0.7	-	-
	7	1.6	-	3.2	-	-	-	0.4	1.2

Table 5.2 Relative energies (in kcal/mol) of $Cr(pyr)_{1+}$ cationic complexes, in different spin states, whose geometries are optimized in theory levels B3LYP, PBE and M06L.

DFT	M	1a	1b	1c	1d	1e	1f	1g	1h
B3LYP	2	-	49.6	-	-	-	46.5	-	49.6
	4	-	34.1	38.7	36.8	30.7	36.3	-	-
	6	2.1	-	3.4	3.0	0.8	**0.0**	-	-
PBE	2	-	35.1	-	-	-	31.4	-	-
	4	-	19.8	-	-	-	16.6	-	-
	6	-	1.9	6.2	-	-	**0.0**	-	-
M06L	2	-	42.2	-	-	54.8	37.4	-	42.2
	4	-	22.3	41.9	-	-	18.5	-	-
	6	-	2.0	6.5	-	-	**0.0**	-	-

The relative energies of the optimized $Cr(pyr)_2$ neutral and cationic complexes in different spin states are presented in Tables 5.3 and 5.4. Some of these structures are shown in Figure 5.3. As seen in Table 5.3, PBE and M06L predict the ground state of $Cr(pyr)_2$ to be a singlet, while B3LYP predicts it to be a quintet. Among the results from the B3LYP calculations, the lowest energy of the singlet complexes is 3.5 kcal/mol. The mismatch between B3LYP and the other two methods can also be seen for the $Cr(pyr)_2^{2+}$ complexes, where B3LYP again predicts the high spin state sextet to have the lowest energy instead of the doublet. Given that the exact HF exchange functional used by B3LYP usually favor higher spin states, it is reasonable to conclude that the ground states of $Cr(pyr)_2$ and $Cr(pyr)_2^{2+}$ are the singlet and doublet, respectively.

The position of the Cr relative to the pyrene and the staggering angles of the two pyrene molecules are two of the factors that affect the energies of the $Cr(pyr)_2^{0/+}$. A chromium can bind to either the α or β ring of each pyrene. The energy difference between the complexes where Cr binds to different rings can be 2-20 kcal/mol. It is shown that the binding of the Cr over the α ring (site *e*, *f* or *g*) is lower in energy, which is consistent with the experiment.[1,2] These energy differences are larger at the lower spin states and smaller at the higher spin states. Especially at the singlet state, which is believed to be the ground spin state, they can be 10-20 kcal/mol. The energies of the structures with small staggering angles are usually lower than those with large staggering angles by less than 6 kcal/mol. Two pyrene molecules can have stronger π-π interactions with small staggering angles, which means the π-π interaction plays a role in stabilizing the complexes. At higher spin states, these the two factors may have similar effects. However, at lower spin states, we can notice that the position of the Cr relative to the pyrene affects the energies more than the staggering angles of the two pyrene molecules.

From Figures 5.2 and 5.3, it is clear that the Cr-pyrene distances in the singlet and doublet structures are shorter than those in the septet and sextet structures, as shown for other Cr-π complexes in the previous chapters. The trend that the Cr-ring distance increases as the spin multiplicity increases is also true for the Cr-pyrene complexes, as it was for the Cr-benzene and the Cr-naphthalene complexes. The distances are longer in the cationic doublet structures than in the neutral singlet structures, which indicates that the electrostatic interaction is not a dominant factor determining the Cr-pyrene bond length. In the high spin states, the Cr-pyrene distance is more than half of the distance between the pyrene planes. As the insertion of a Cr pushes two pyrene molecules apart at the Cr end, the π-π interaction tries to pull the two planes together at the other end. Therefore, the two pyrene molecules are not parallel but are tilted like a clamp to flank the Cr. In the high spin states, the openings of the "clamps" are bigger because the Cr-pyrene distances are longer.

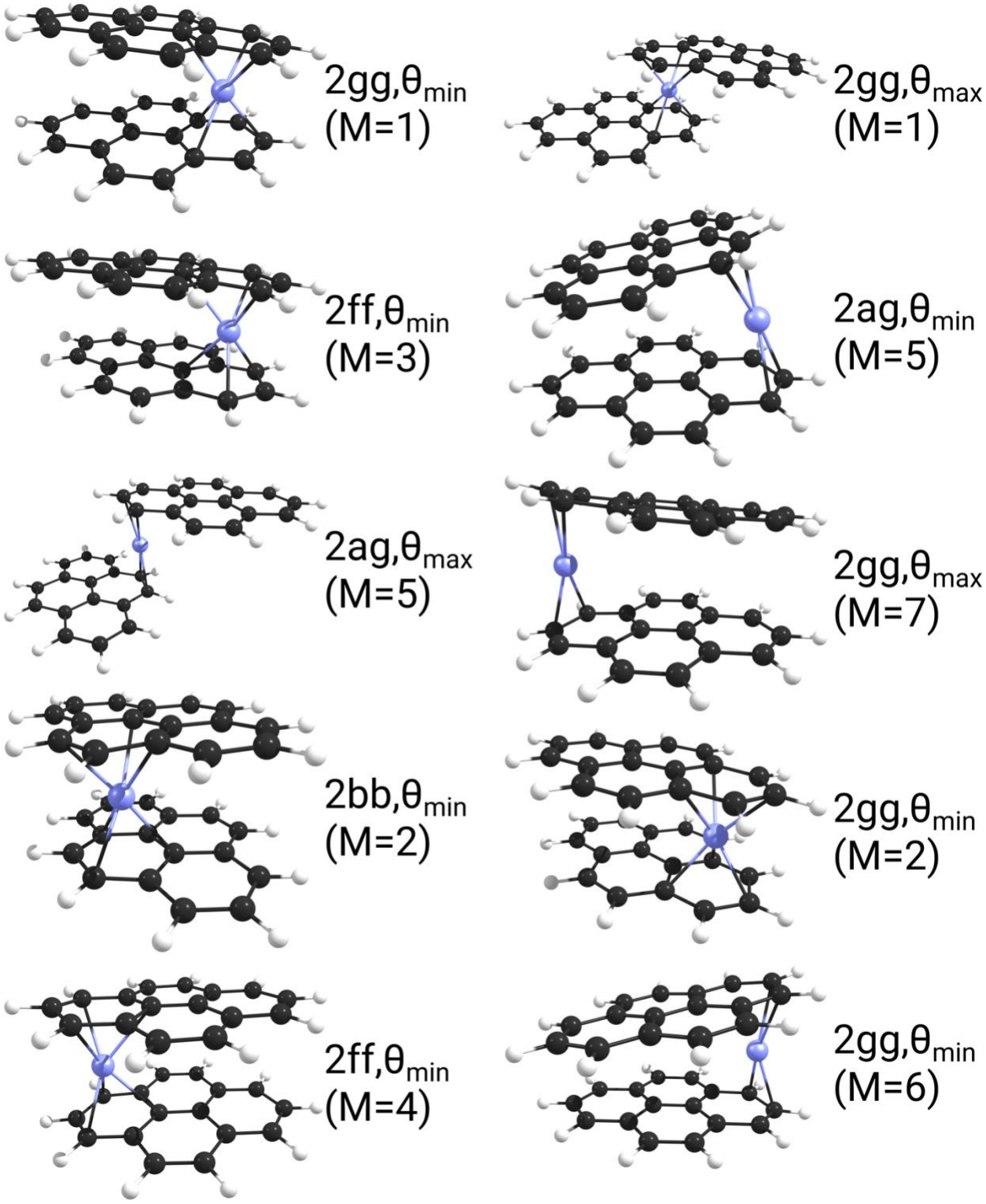

Figure 5.3 Selected $Cr(pyr)_2$ structures in neutral (M=1,3,5,7) and cationic (M=2,4,6) forms.

Table 5.3 Relative energies (in kcal/mol) of $Cr(pyr)_2$ neutral complexes, in different spin states, whose geometries are optimized in theory levels B3LYP, PBE and M06L. θ_{min} (or θ_{max}) indicates that two pyrene molecules have small (or large) staggering angles.

DFT	M	2aa,θ_{min}	2bb,θ_{min}	2af,θ_{min}	2bf,θ_{min}	2ag,θ_{min}	2ff,θ_{min}	2gg,θ_{min}	2aa,θ_{max}	2bb,θ_{max}	2bf,θ_{max}	2ag,θ_{max}	2ff,θ_{max}	2gg,θ_{max}
B3LYP	1	-	23.3	-	14.4	-	3.5	-	-	27.2	18.1	-	9.8	-
	3	-	19.1	17.3	-	-	15.4	-	-	-	19.8	-	17.6	-
	5	-	29.8	-	-	**0.0**	-	4.5	5.9	-	-	7.6	-	10.9
	7	4.5	-	-	-	2.6	-	-	11.7	-	-	12.5	-	-
PBE	1	-	21.1	-	11.2	-	**0.0**	-	-	19.8	13.3	-	5.2	-
	3	-	18.0	-	16.7	-	13.5	-	-	20.5	19.4	-	17.4	-
	5	-	31.9	25.3	-	-	-	22.1	26.0	-	-	24.7	-	26.1
	7	32.5	-	-	-	29.8	-	29.8	37.8	-	-	36.8	-	36.4
M06L	1	-	19.4	-	10.9	-	**0.0**	-	-	20.4	13.9	-	5.8	-
	3	-	14.0	-	14.5	-	11.3	-	-	17.5	17.5	-	14.4	-
	5	11.0	-	12.2	-	-	-	-	14.9	-	-	14.0	-	15.1
	7	17.6	-	-	-	15.1	-	14.8	23.2	-	-	22.7	-	22.4

Table 5.4 Relative energies (in kcal/mol) of $Cr(pyr)_2^{2+}$ cationic complexes, in different spin states, whose geometries are optimized in theory levels B3LYP, PBE and M06L. θ_{min} (or θ_{max}) indicates that two pyrene molecules have small (or large) staggering angles.

DFT		2aa,θ_{min}	2bb,θ_{min}	2af,θ_{min}	2bf,θ_{min}	2ag,θ_{min}	2ff,θ_{min}	2gg,θ_{min}	2aa,θ_{max}	2bb,θ_{max}	2bf,θ_{max}	2ag,θ_{max}	2ff,θ_{max}	2gg,θ_{max}
B3LYP	M=2	-	34.3	-	26.9	-	33.2	-	-	36.0	32.9	-	38.7	-
	M=4	-	26.8	24.4	-	-	18.8	-	-	27.3	28.3	-	-	23.4
	M=6	3.0[a]	-	-	-	1.0	-	**0.0**	8.8	-	-	-	-	2.4[b]
PBE	M=2	-	21.4	-	10.4	-	**0.0**	-	-	20.1	13.2	-	5.1	-
	M=4	-	18.2	-	18.0	-	17.8	-	-	19.2	17.6	-	21.5	-
	M=6	19.0	-	-	-	16.4	-	14.5	22.9	-	-	-	-	-
M06-L	M=2	-	19.7	-	10.6	-	**0.0**	-	-	21.0	14.3	-	6.5	-
	M=4	-	12.2	-	11.7	-	8.4	-	-	12.6	14.3	-	13.3	-
	M=6	4.8	-	-	-	2.2	-	0.5	-	-	-	8.1	-	6.1

[a] 2ah,θ_{min}

[b] 2eg,θ_{min}

Binding Energies

The dissociation of $Cr(pyr)_2^{0/+}$ complexes may be composed of two consecutive steps. The first is the loss of pyrene:

$$Cr(pyr)_2^{0/+} \rightarrow Cr(pyr)_1^{0/+} + pyr$$

According to the results shown later, the ionization potential of $Cr(pyr)_1$ is much lower than the 7.43 eV value of pyrene. Therefore, after the dissociation of $Cr(pyr)_2^{+}$, the charge should stay on the metal complex instead of on the pyrene. The second step is the loss of the other pyrene, which equals the dissociation of $Cr(pyr)_1^{0/+}$:

$$Cr(pyr)_1^{0/+} \rightarrow Cr^{0/+} + pyr$$

The ionization potential of Cr is about 6.77 eV, which is lower than that of pyrene. So the cationic $Cr(pyr)_1^{+}$ dissociates into a Cr^{+} cation and a neutral pyrene. Calculated binding energies of Cr to pyrene are shown in Table 5.5, including binding to the first, the second, and both pyrenes, which are represented by B.E.1, B.E.2, and B.E.sum, respectively. Both the results with the Wigner-Witmer spin conservation rules (M=M´),[10] and with the spin cross over (M≠M´) are shown here.

M is the spin multiplicity of the Cr complex with more pyrene ligands, namely the spin multiplicity of a bare Cr for B.E.1 and B.E.sum, and the spin multiplicity of the $Cr(pyr)_1^{0/+}$ for B.E.2. When the spin cross over is taken into account, the multiplicity of the Cr complex with fewer pyrene ligands (M´) is set to be its ground spin state predicted by computations. In most cases, M´=7 is chosen for Cr atom and $Cr(naph)_1$, and M´= 6 for Cr^{+} and $Cr(pyr)_1^{+}$. An exception is the results of B.E.2 with M06L, since M06L predicts the ground spin state of the

$Cr(pyr)_1$ to be a quintet, as seen in Table 5.1. B.E.1 values with the spin cross-over ($M \neq M'$) are negative for the neutral complexes in the lower spin states (M = 1 or 3). This indicates that the flip of the electron spins costs more energy than that released from the formation of the first Cr-pyrene bond. The spin cross-over energy is also the reason why the binding energies with the spin conservation rules are always higher than those without, which is observed in Table 5.5.

The binding energies computed for the pyrene complexes are compared to those computed for the benzene and naphthalene complexes shown in previous chapters. The binding energies B.E.1 with $M = M' = 6$ or 7 are higher for the Cr-pyrene complexes than those for the benzene or pyrene complexes, as predicted by each of the three DFT methods used in this study. All three DFT methods agree that the B.E.2 of the neutral Cr-pyrene with $M = M' = 1$ is larger than that of the corresponding Cr-benzene or Cr-naphthalene complex. The B.E.2 values of the cationic Cr-pyrene complexes with $M = M' = 2$ given by the three methods are higher than the B.E.2 of the corresponding Cr-naphthalene complexes. On the other hand, both B3LYP and PBE predict that the B.E.2 of $Cr(pyr)^{2+}$ is lower than that of the $Cr(bz)^{2+}$, except that M06L alone predicts a higher value. This finding of a stronger Cr-pyrene bond contradicts the proposition from the ligand-exchange experiments that the binding strength of Cr to the arene follows the order of benzene > naphthalene > pyrene.[4,11] In the ligand-exchange experiments, the complexes had two or more ligands on Cr, and the reactions only substitute one of the ligands. Therefore, the trend found in those experiments may not be relevant to the B.E.1 and B.E.2 results in this study.

Table 5.5 Bond energies (kcal/mol) of Cr binding to the first (B.E.1), the second (B.E.2), and both (B.E.sum) pyrene molecules, with (M≠M') and without (M=M') spin cross over. B.E.x = $E[Cr(pyr)_{x\text{-}10/+}] + E[pyr] - E[Cr(pyr)_{x0/+}]$. B.E.sum = $E[Cr_{0/+}] + 2E[pyr] - E[Cr(pyr)_{20/+}]$.

		B.E.1		B.E.2		B.E.sum	
	M´	M=M´	M≠M´	M=M´	M≠M´	M=M´	M≠M´
B3LYP	1	54.2	-50.9	80.3	19.8	134.5	29.5
	3	20.7	-29.8	47.4	7.9	68.1	17.6
	5	13.6	-4.3	37.3	23.3	50.9	33.0
	7	9.7	-	20.7	-	30.4	-
	2	56.2	1.1	67.0	18.3	123.1	68.1
	4	54.9	15.6	60.6	26.5	115.5	76.2
	6	49.8	-	44.8	-	94.6	-
PBE	1	42.7	-26.7	91.7	57.7	134.3	65.0
	3	45.1	-12.4	64.0	44.3	109.1	51.5
	5	31.2	3.4	39.5	35.7	70.8	42.9
	7	7.3	-	28.0	-	35.2	-
	2	80.7	21.9	94.5	62.3	175.1	116.4
	4	78.3	37.6	61.2	44.7	139.5	98.8
	6	54.1	-	47.7	-	101.9	-
M06L	1	95.3	-15.8	78.9	54.5	174.2	63.0
	3	39.1	-11.8	63.5	43.2	102.6	51.7
	5	22.2	8.6	44.2	-	66.4	52.7
	7	8.2	-	40.0	39.6	48.2	-
	2	76.8	15.5	92.7	53.5	169.5	108.1
	4	77.5	36.1	63.7	45.1	141.2	99.7
	6	54.6	-	53.0	-	107.6	-

Ionization Potentials

The calculated vertical and adiabatic ionization potentials (IP_v and IP_a) are presented in Table 5.6. The selection rule for the multiplicity change of $\Delta M=1$ is applied here. For vertical ionization, the structures of cations are inherited from the neturals. Since the lowest energy computed by M06L for the neutral $Cr(pyr)_1$ is a quintet, the IP_a is evaluated as the $M=6\leftarrow5$ transition. In the same manner, the IP_a of $Cr(pyr)_2$ computed by B3LYP is evaluated as the $M=6\leftarrow5$ transition. The IP_v values are compared to those of the corresponding benzene complexes and naphthalene complexes shown in Tables 3.4 and Table 4.5. The ionization potentials of $^{6\leftarrow7}Cr(pyr)_1$ and $^{2\leftarrow1}Cr(pyr)_2$ are smaller than those of the corresponding Cr-naphthalene complexes, and are thus also smaller than those of the corresponding Cr-benzene complexes. This is probably because pyrene has a larger conjugated π system to stabilize the cations of the Cr naphthalene complexes.

Summary

There is a slight preference for the Cr to bind to the α ring of pyrene. The energy differences are not significant for the $Cr(pyr)_{1+}$ complexes. However, the effect of the binding position of the Cr on pyrene is more important than that of the staggering angles of the two pyrene molecules, even though the π-π interaction contributes to the stability of the complexes. It is shown that the $Cr(pyr)_{2}^{0/+}$ complexes energetically prefer the lowest spin state and the $Cr(pyr)_{1}^{0/+}$ complexes prefer the highest spin state. Inconsistent results about the ground state spin are given by M06L for $Cr(pyr)_1$ and by B3LYP for $Cr(pyr)_2$, where the quintet is predicted to be the ground state. Since the high spin states have longer Cr-ring distances and the π-π interaction between two pyrene molecules trends to make them closer to each other, the structures of the $Cr(pyr)_{2}^{0/+}$

complexes with small staggering angles are like clamps with Cr in the opening. This is especially obvious for the complexes in the high spin states. The computed binding energies indicate that pyrene generally binds weaker to Cr than benzene or naphthalene, which does not agree with the experimentally determined order of bond strength for arenes including benzene, naphthalene, and pyrene.[4,11] The Cr-pyrene complexes have lower ionization potentials than the Cr-naphthalene complexes, and are thus even lower than those of the Cr-benzene complexes, which supports the hypothesis that the larger PAH provides a larger conjugated π systems to stabilize the cations.

Table 5.6 Vertical ionization potentials (IP_v) and adiabatic ionization potentials (IP_a) of $Cr(pyr)_x$ complexes in the unit of eV, where the spin multiplicity change is limited to $\Delta M=\pm 1$ in vertical ionizations. M is the spin multiplicity of a neutral complex, and M´ is the spin multiplicity of a cationic complex.

			PBE		B3LYP		M06-L	
Complex	M	M´	IPv	IPa	IPv	IPa	IPv	IPa
	1	2	5.36		5.08		5.50	
	3	2	5.82		5.95		5.69	
x=1	3	4	5.33		5.17		4.84	
	5	4	6.33		6.36		6.22	
	5	6	5.59		5.16		5.32	4.84
	7	6	5.52	5.23	5.56	5.20	5.09	
	1	2	5.07	5.04	4.92		4.94	4.88
	3	2	4.61		5.06		4.78	
x=2	3	4	5.58		4.78		5.01	
	5	4	5.07		5.54		5.07	
	5	6	5.16		4.49	4.27	4.70	
	7	6	4.55		4.29		4.42	

References

(1) Peitz, D. J.; Palmer, R. T.; Radonovich, L. J.; Woolsey, N. F. Preparation and Structure of (μ-Phenanthrene)- and (μ-Pyrene)Bis(Tricarbonylchromium). *Organometallics* **1993**, *12*, 4580–4584.

(2) Arrais, A.; Diana, E.; Gervasio, G.; Gobetto, R.; Marabello, D.; Stanghellini, P. L. Synthesis, Structural and Spectroscopic Characterization of Four [(η_6-PAH)$Cr(CO)_3$] Complexes (PAH = Pyrene, Perylene, Chrysene, 1,2-Benzanthracene). *Eur. J. Inorg. Chem.* **2004**, 1505–1513.

(3) Kurikawa, T.; Takeda, H.; Hirano, M.; Judai, K.; Arita, T.; Nagao, S.; Nakajima, A.; Kaya, K. Electronic Properties of Organometallic Metal−Benzene Complexes [M_n(Benzene)$_m$ (M = Sc−Cu)]. *Organometallics* **1999**, *18*, 1430–1438.

(4) Howell, J. A. S.; Ashford, N. F.; Dixon, D. T.; Kola, J. C.; Albright, T. A.; Kang, S. K. The Arene-Exchange Reaction in Naphthalene- and Pyrene-$Cr(CO)_3$. *Organometallics* **1991**, *10*, 1852–1864.

(5) Elustondo, F.; Dalibart, M.; Deroult, J.; Mascetti, J. Matrix Isolation Spectroscopy Study of Iron Reactivity towards PAHs. *Phys. Chem. Earth, Part C Solar, Terr. Planet. Sci.* **1999**, *24*, 583–589.

(6) Scott, A. C.; Buchanan, J. W.; Flynn, N. D.; Duncan, M. A. Photodissociation of Iron-Pyrene and Iron-Perylene Cation Complexes. *Int. J. Mass Spectrom.* **2007**, *266*, 149–155.

(7) Simon, A.; Joblin, C. Thermochemistry and Infrared Spectroscopy of Neutral and Cationic Iron−Polycyclic Aromatic Hydrocarbon Complexes of Astrophysical Interest: Fundamental Density Functional Theory Studies. *J. Phys. Chem. A* **2007**, *111*, 9745–9755.

(8) Wang, Y.; Szczepanski, J.; Vala, M. Vibrational Spectroscopy of Neutral Complexes of

Fe and Polycyclic Aromatic Hydrocarbons. *Chem. Phys.* **2007**, *342*, 107–118.

(9) Scott, A. C.; Buchanan, J. W.; Flynn, N. D.; Duncan, M. A. Photodissociation Studies of Calcium–Coronene and Calcium–Pyrene Cation Clusters. *Int. J. Mass Spectrom.* **2008**, *269*, 55–61.

(10) Wigner, E.; Witmer, E. E. Über Die Struktur Der Zweiatomigen Molekelspektren Nach Der Quantenmechanik. *Zeitschrift für Phys.* **1928**, *51*, 859–886.

(11) Bush, B. F.; Lynch, V. M.; Lagowski, J. J. Transition-Metal Organometallic Compounds: 8: Arene Exchange Reactions of Bis(Naphthalene)Chromium. *Organometallics* **1987**, *6*, 1267–1275.

CHAPTER 6

STRUCTURES AND ENERGETICS OF CHROMIUM CORONENE COMPLEXES PREDICTED BY DFT CALCULATIONS

Introduction

Coronene is a PAH with six fused benzene rings with D_{6h} symmetry. Its interior ring is a good prototype for rings in carbon materials such as graphene and carbon nanotubes. For this reason coronene is often used as a model representing a finite section of a carbon surface. Therefore, studying the interactions between transition metals and coronene is an important step towards understanding transition metals supported on graphene or other carbon materials.

Cationic transition metal coronene complexes in the gas phase were first described by Dunbar and co-workers.[1,2] The first chromium coronene cationic complexes made by the laser vaporization with the supersonic expansion cooling were reported by Duncan and co-workers.[3] They confirmed the multidecker sandwich structures for the $Cr_m(coronene)_n^+$ complexes, and the possibility for one coronene to coordinate up to three chromium atoms. Duncan and co-workers later detected chromium coronene cationic complexes with a mass spectrometer from the laser vaporization of the mixed powder containing metal and coronene without cooling.[4] This experiment indicated that chromium coronene complexes are stable enough not to decompose under the hot laser vaporization condition. However, no one has claimed to successfully isolate complexes as these. The competitive binding and photodissociation studies performed by Duncan and co-workers suggest that the binding strengths of metals with coronene are higher than those with benzene and C_{60}.[5] This is consistent with the theory studies by Klippenstein and

co-workers.[2] More theory work on TM-PAH complexes has been done by Dunbar, Jena and their co-workers.[6,7]

A few theory studies on chromium-coronene complexes were published. Philpott *et al.* performed DFT calculations for Cr_7(coronene)$_2$ and found its lowest energy state has the electron spin S=5.[8] Türker *et al.* did DFT studies on the η^6-coronene-$Cr(CO)_3$ complexes to demonstrate that Cr prefers to bind to the peripheral rings of coronene.[9] This is in agreement with the hypotheses proposed by many other theoreticians that the electron density over the peripheral rings is higher than that over the interior ring, so that transition metals acting as electron acceptors prefer to bind on the peripheral rings. Yu and co-workers studied Cr(coronene)$_2$ complexes treating the chromium atom as a spacer between two face-to-face stacked coronene molecules.[10] In their result, the lowest energy structure is a singlet that has the chromium between the two peripheral rings. However, they fixed the coronene molecules in the face-to-face position, which means the structures of the complexes were restricted to D_{6h} or C_{2v}. The structures with one of the coronene molecules rotating about the metal atom in parallel to the other coronene have not been studied. This chapter discusses the results from DFT calculations on the chromium-coronene complexes including additional structural possibilities.

Model Setup

Given the symmetry, There are six chemically different η^6 and η^2 binding sites on a coronene surface, as shown in Figure 6.1. Geometry optimizations of Cr(cor)$_1$ (cor=coronene) start with structures where Cr binds to those sites. The optimized structure may have Cr sitting directly above one carbon, in a σ-bonded configuration. In these cases, structures are named as their closest η^2-bonded structures. The nomenclature for Cr(cor)$_1$ complexes takes the form of *1b*,

where 1 represents the number of coronene and *b* indicates where the Cr sits over the coronene. An example of bonding in *1c* configuration is shown in Figure 6.1.

When there are two coronene molecules facing each other with a sandwiched Cr, The structures can vary not only with the different Cr-binding sites on each coronene, but also with the angle of the coronenes with respect to each other. The structures are named following the pattern as *2cc,*$\theta_{min.}$ 2 means there are two coronene molecules. Cr is over the site *c* of each coronene. In addition, θ_{min} indicates that the staggering angles of two coronene molecules are close to 0°, where they can have the most π-π interaction. Three examples of $Cr(cor)_2$ complexes are shown in Figure 6.1.

The geometry optimizations of the $Cr(cor)_{1}^{0/+}$ complexes start with the six structures from *1a* to *1f* respectively for each spin state. For the $Cr(cor)_{2}^{0/+}$ complexes, the geometry optimizations start with the Cr at the positions *2aa*, *2cc*, and *2ac*. The staggering angles are set to 15° and 180° at the beginning of the calculations, but it is simplified to θ_{min} and θ_{max} in the results.

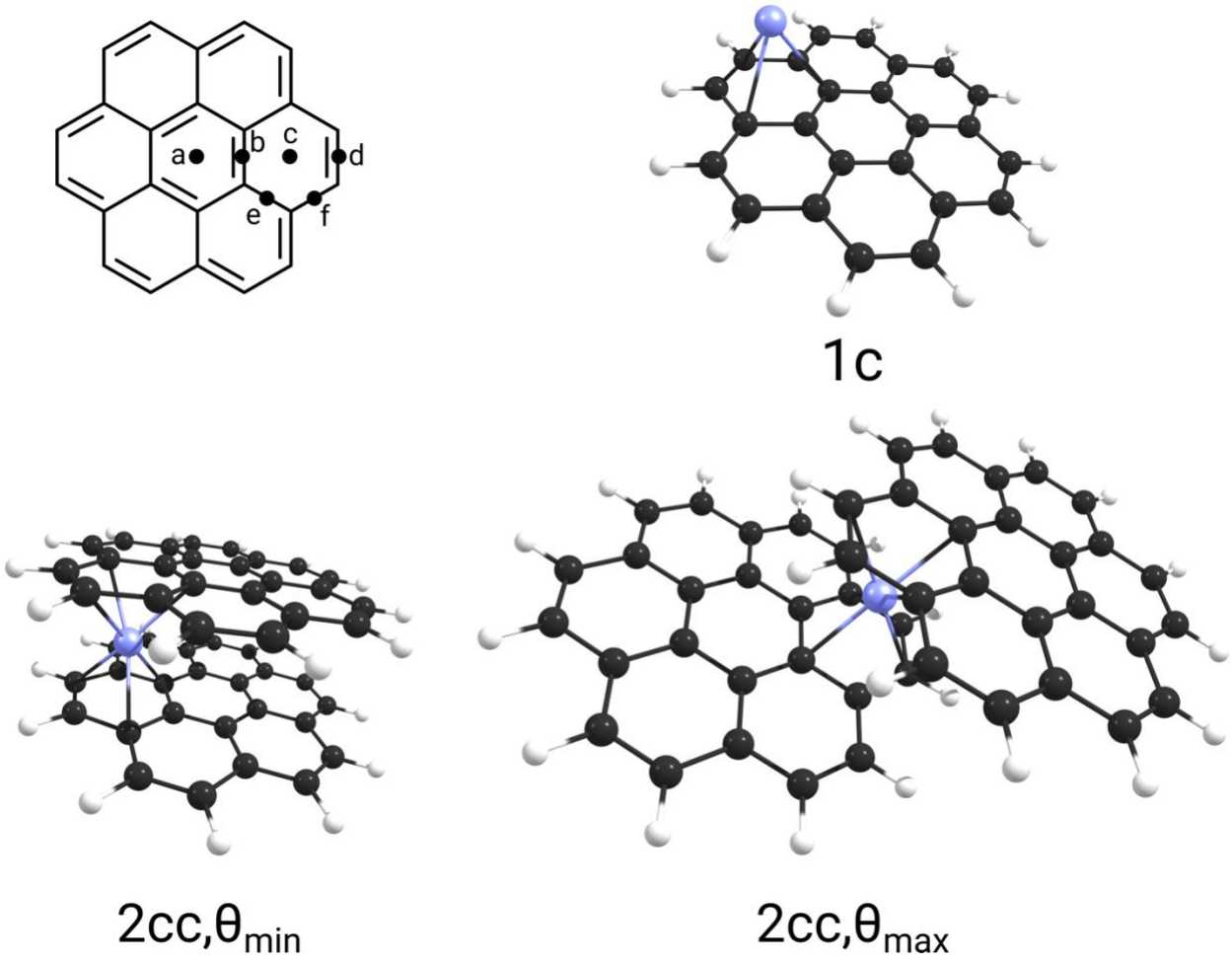

Figure 6.1 Possible binding sites on coronene and Cr-coronene complexes.

Geometries and Spin Multiplicities

Previous experiments suggested a sandwich structure for the $Cr(cor)_2$.[3] However, no existing experiment has determined the structure yet. The computed relative energies from this study for the $Cr(cor)_{1}^{0/+}$ complexes with Cr binding on different sites are shown in Tables 6.1 and 6.2. Some of the optimized structure are presented in Figure 6.2. It can be seen from the tables that the $Cr(cor)_{1}^{0/+}$ complexes prefer high spin states, namely the septet (M = 7) for the neutral complexes and the sextet (M = 6) for the cationic complexes. For the neutral $Cr(cor)_1$, the energies of the quintet complexes are higher than that of the ground spin state (M = 7) by 6.0 and 1.6 kcal/mol as predicted by PBE and M06L, respectively. Considering the common error of DFT calculations, M06L results suggest both either the quintet or septet is possibly the ground state spin, but the other two methods agree that the septet is the ground state spin for the $Cr(cor)_1$. For the cationic $Cr(cor)_1^+$, the three methods agree that the ground state spin is the sextet. One possible explanation for the preference for the high spin state is that the spin cross-over is energy consuming, while the energy of the coordination of one PAH molecule is not large enough to compensate for it. Therefore, the single coordinated $Cr(PAH)_1$ usually adopts the high spin state.

The $Cr(cor)_{1}^{0/+}$ complexes have longer Cr-ring distances in the higher spin states, as seen for the Cr-benzene, Cr-naphthalene, and Cr-pyrene complexes. This is consistent in all three DFT methods used in this study. The Cr-ring distance is longer as a doublet than that as a singlet, even though the singlet Cr is neutral and the doublet Cr is cationic. Therefore, it is believed that the electrostatic interaction is not a dominant force to determine the Cr-coronene bond length.

For the lower spin states (M < 5), it is shown in the tables that the energy differences between structures that have the Cr binding on different sites are large enough to distinguish the preferred Cr binding sites on coronene. However, these differences are small (< 3 kcal/mol) for the higher spin states (M ≥ 5). If the $Cr(cor)_1$ complexes are in their ground spin states, either the septet or the sextet, it is hard to tell which of the six sites the Cr prefers. The site preference may be influenced by the d-π interaction involved in the Cr-coronene bond. It is known that the strength of the d-π interaction is proportional to the reverse of the distance.[11] As a result, the d-π interaction is weaker in the higher spin states, since the distance is longer. The change of the ligand field, in turn, has less impact on the energies of the complexes. Nevertheless, both PBE and M06L predict that the septet $Cr(cor)_1$ prefers the *1d* structure, and only B3LYP predicts that *1b* is favored. Additionally, the sextet $Cr(cor)_{1+}$ prefers the *1c* structure, as predicted by all three methods. In all of these cases, the calculations in this study agree that the Cr prefers to bind to the peripheral ring of coronene, as proposed in previous studies.

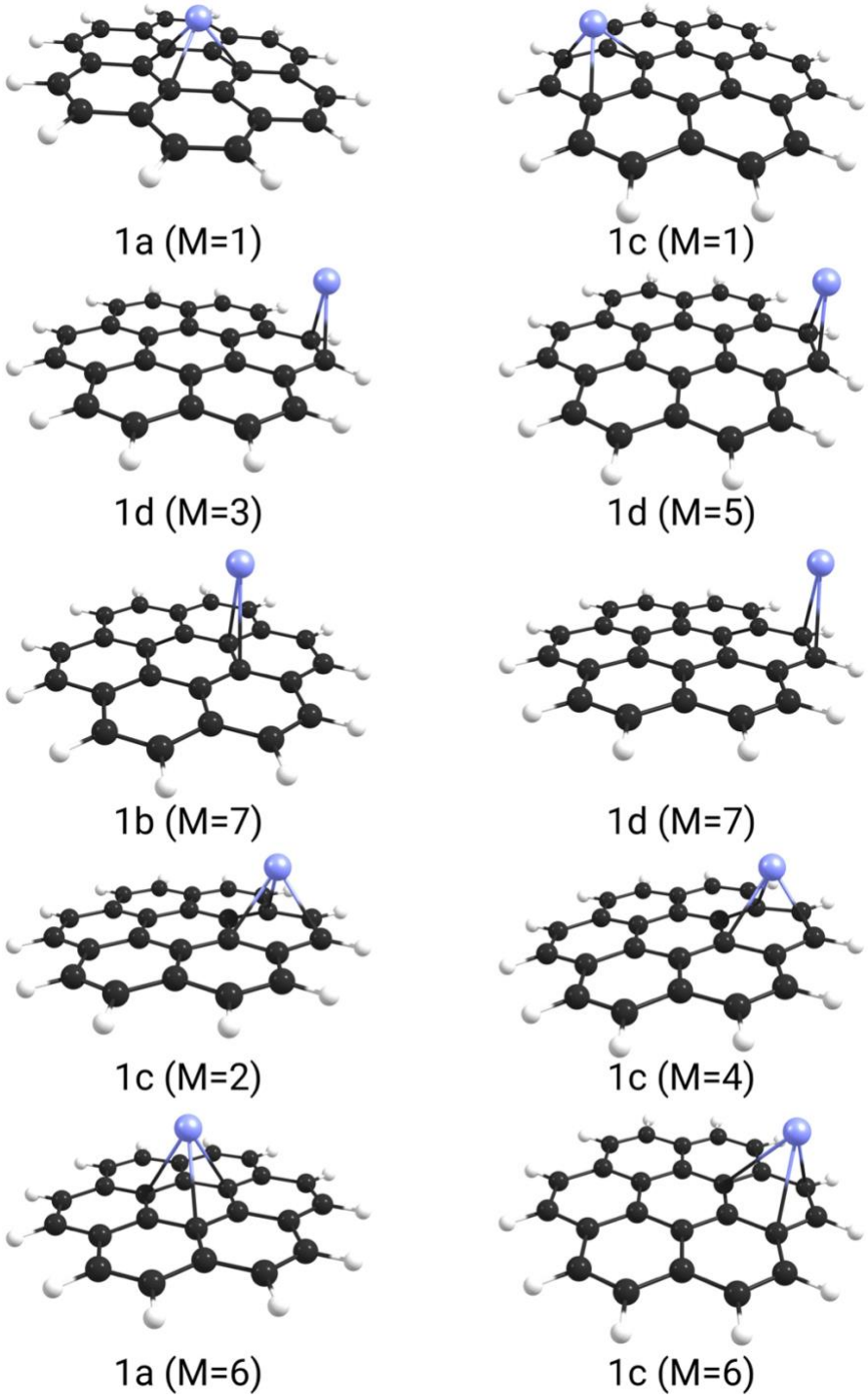

Figure 6.2 Selected $Cr(cor)_1$ structures in neutral (M=1,3,5,7) and cationic (M=2,4,6) forms.

Table 6.1 Relative energies (in kcal/mol) of $Cr(cor)_1$ neutral complexes, in different spin states, whose geometries are optimized in theory levels B3LYP, PBE and M06L.

DFT	M	1a	1b	1c	1d	1e	1f
B3LYP	1	78.9	-	60.0	-	-	-
	3	49.0	51.2	-	43.3	49.5	-
	5	-	15.8	-	15.4	16.1	16.2
	7	-	**0.0**	-	-	-	-
PBE	1	45.1	-	28.7	-	-	-
	3	40.1	-	24.3	32.7	-	-
	5	-	23.3	-	6.0	-	-
	7	-	1.1	-	**0.0**	-	-
M06L	1	50.3	-	30.2	-	-	-
	3	41.8	-	23.1	31.4	-	-
	5	-	11.7	2.2	1.6	10.7	-
	7	1.6	1.3	-	**0.0**	-	-

Table 6.2 Relative energies (in kcal/mol) of $Cr(cor)_{1+}$ cationic complexes, in different spin states, whose geometries are optimized in theory levels B3LYP, PBE and M06L.

DFT	M	1a	1b	1c	1d
B3LYP	2	52.2	-	47.1	-
	4	43.8	36.5	32.7	32.7
	6	1.6	1.6	**0.0**	-
PBE	2	45.8	-	32.7	-
	4	32.5	-	19.2	-
	6	2.4	-	**0.0**	-
M06L	2	52.6	-	38.8	-
	4	36.6	-	21.8	-
	6	2.8	-	**0.0**	-

The computed relative energies of the $Cr(cor)_2^{0/+}$ complexes from this study where the Cr binds on different sites and the coronene molecules have different staggering angles are shown in Tables 6.3 and 6.4. Some of the optimized structure are presented in Figure 6.3. The different DFT methods cannot agree on the ground state spins for either the $Cr(cor)_2$ or the $Cr(cor)_2^{2+}$. The calculations with B3LYP suggest that the ground state for the $Cr(cor)_2$ is a septet instead of a singlet as predicted by PBE and M06L. It is not surprising that B3LYP predicts the high spin states to be the more stable for we have seen in previous chapters that B3LYP overstabilizes the high spin complexes. Additionally, M06L predicts the high spin sextet to be the ground state for $Cr(cor)_2^{2+}$, which is not common in previous studies with other PAHs. Based on the previous experience, PBE is usually reliable to predict the ground state spins. Thus, it is tempting to conclude that the doublet is the ground state of $Cr(cor)_2^{2+}$. However, we cannot not be sure which spin state has the lowest energy based only on these calculations. Experimental measurements of the spin multiplicities would be necessary to determine their ground state spins.

As in the Cr-PAH complexes we have discussed previously, the Cr-ring distance in the $Cr(cor)_2^{0/+}$ increases with the spin multiplicity. The Cr-ring distance in the singlet spin state is shorter than a half of the distance between two coronene molecules. Hence we can see in Figure 6.3 that the singlet $2cc,\theta_{min}$ structure has the two coronene molecules tilted towards the Cr. However, in the higher spin states, the Cr atoms push the flanking coronene molecules apart, thus the complexes have scissors-like structures with the Cr in the openings. The tilt is attributed to the π-π interaction between the coronene molecules. The effect of the π-π interaction can be noticed from the energies differences between the structures with different staggering angles. The energies with the smaller staggering angles, that is with more π-π interaction, are usually higher than those with less π-π interaction by over 7 kcal/mol. The energy differences for the

Cr-coronene complexes due to the π-π interaction are larger than those for the complexes of naphthalene and pyrene. The differences are less than 6 kcal/mol for the $Cr(pyr)_2$ complexes and even lower for the $Cr(naph)_2$ complexes. This is because the coronene has a larger conjugated π system than the other PAHs which are mentioned in the previous chapters. Therefore the π-π interaction plays a more important role in the stability of Cr-coronene complexes.

The Cr is not always binding to the η_6 sites on the coronene, as seen from Figures 6.2 and 6.3. In higher spin states, the Cr is more likely binding to the η_2 sites instead of the η_6 sites. $Cr(cor)_1$ with the spin multiplicity M = 3, 5, or 7 prefers the *1b* or *1d* structures. Although the structure of the sextet $Cr(cor)_{1+}$ with the lowest energy is named as *1c*, the Cr is actually in a position between *c* and *d*, which indicates that it is not η_6-coordinated, but is instead η_2- or η_4-coordinated. The same phenomenon is seen for the di-coronene complexes. In the lower spin state, namely M = 1, 2, 3, or 4, the Cr prefers to bind to the coronene over the centroid of the peripheral ring. However, the $Cr(cor)_{2}^{0/+}$ complexes in higher spin states adopt the structures like *2dd*, *2bd*, and *2ad*, with the Cr over the C-C bonds instead of the centroid of the ring. This discovery is consistent with the result from a previous theory study, which found that the Cr prefers to bind over the outermost C-C bond for the quintet and the septet.[10]

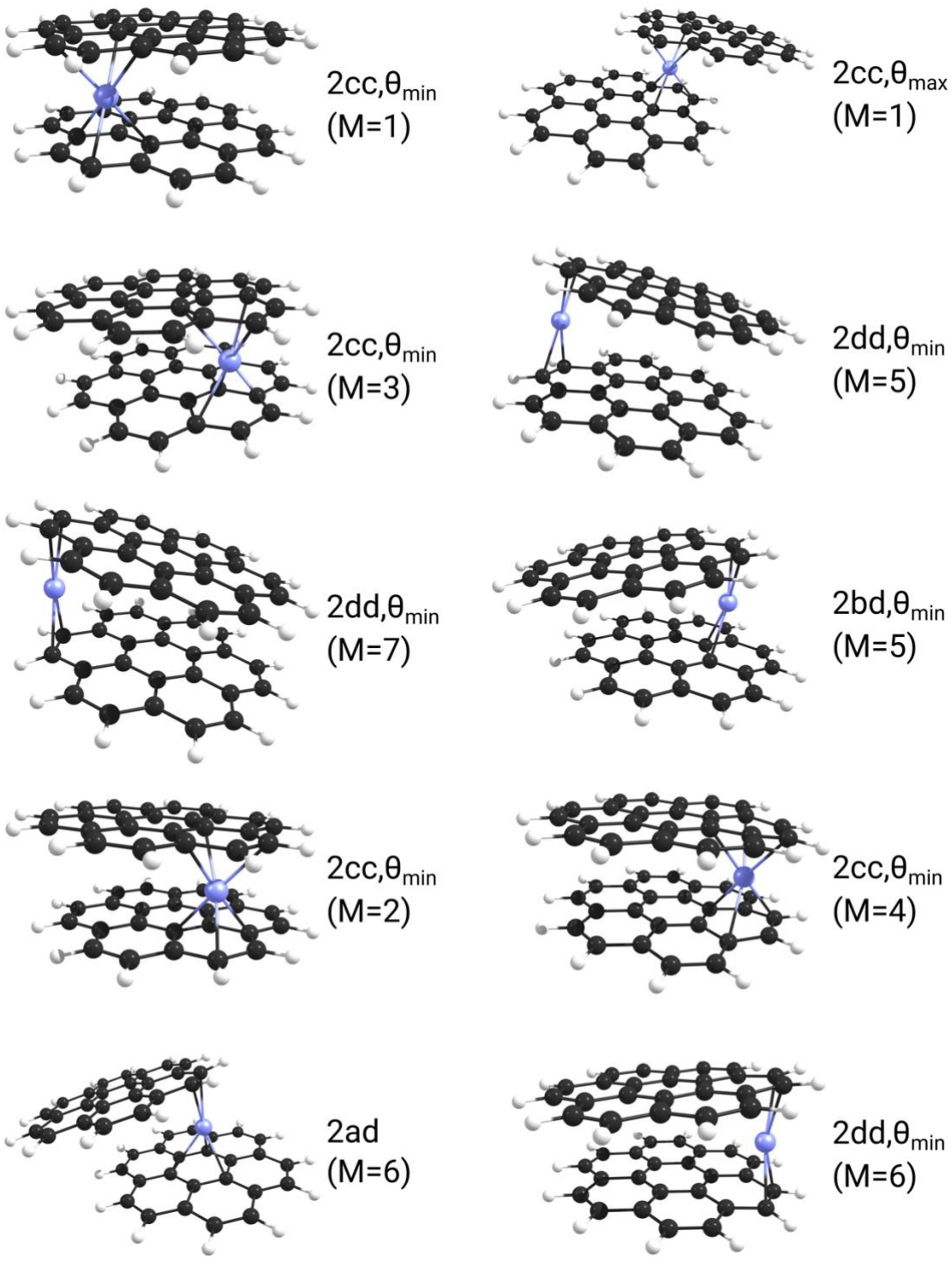

Figure 6.3 Selected $Cr(cor)_2$ structures in neutral (M=1,3,5,7) and cationic (M=2,4,6) forms.

Table 6.3 Relative energies (in kcal/mol) of $Cr(cor)_2$ neutral complexes, in different spin states, whose geometries are optimized in theory levels B3LYP, PBE and M06L. θ_{min} (or θ_{max}) indicates that two coronene molecules have small (or large) staggering angles.

DFT	M	2aa	2ac	2bd,θ_{min}	2cc,θ_{min}	2dd,θ_{min}	2cc,θ_{max}	2dd,θ_{max}
B3LYP	1	32.8	19.4	-	5.8	-	15.3	-
	3	40.4	26.5	-	10.6	-	23.0	-
	5	30.3	-	5.0	-	0.2	-	7.4
	7	18.0	-	6.8	-	**0.0**	-	14.9
PBE	1	27.0	13.7	-	**0.0**	-	7.9	-
	3	35.2	20.7	-	7.1	-	15.2	-
	5	34.8	-	24.7	19.2	-	-	21.9
	7	38.7	-	32.4	-	25.7	-	36.0
M06L	1	30.3	16.2	-	**0.0**	-	10.9	-
	3	36.5	21.0	-	4.8	-	16.2	-
	5	27.1	-	12.5	8.5	-	-	13.4
	7	25.3	-	19.9	-	11.9	-	24.3

Table 6.4 Relative energies (in kcal/mol) of $Cr(cor)_2^{2+}$ cationic complexes, in different spin states, whose geometries are optimized in theory levels B3LYP, PBE and M06L. θ_{min} (or θ_{max}) indicates that two pyrene molecules have small (or large) staggering angles.

DFT	M	2aa	2ac	2ad	2cc,θ_{min}	2dd,θ_{min}	2cc,θ_{max}	2dd,θ_{max}
B3LYP	2	49.4	38.7	-	26.5	-	37.7	-
	4	45.2	34.9	-	24.4	-	33.6	-
	6	13.6	-	7.9[a]	-	**0.0**	-	13.6
PBE	2	27.5	14.0	-	**0.0**	-	7.8	-
	4	30.6	18.9	-	7.9	-	14.8	-
	6	18.0	-	12.3	-	6.4	-	17.1
M06L	2	37.8	24.3	-	7.7	-	18.7	-
	4	32.2	20.1	-	8.8	-	17.0	-
	6	11.2	-	5.7	-	**0.0**	-	12.8

[a] 2bd,θ_{min}

Binding Energies

The dissociation of $Cr(cor)_2^{0/+}$ complexes may be composed of two consecutive steps. The first is the loss of coronene:

$$Cr(cor)_2^{0/+} \rightarrow Cr(cor)_1^{0/+} + cor$$

According to the results shown later, the ionization potential of $Cr(cor)_1$ is much lower than the 7.29 eV value of coronene. Therefore, after the dissociation of $Cr(cor)_2^+$, the charge should stay on the metal complex instead of on the coronene. The second step is the loss of the other coronene, which equals the dissociation of $Cr(cor)_1^{0/+}$:

$$Cr(cor)_1^{0/+} \rightarrow Cr^{0/+} + cor$$

The ionization potential of Cr is 6.77 eV, which is lower than that of coronene (7.29 eV). So the cationic $Cr(cor)_1^+$ dissociates into a Cr^+ cation and a neutral coronene. Calculated binding energies of Cr binding to coronene are shown in Table 6.5, including binding to the first, the second, and both coronene molecules, which are represented by B.E.1, B.E.2, and B.E.sum, respectively. Both the results with the Wigner-Witmer spin conservation rules (M=M´),[12] and with the spin-cross over (M≠M´) are shown here.

M is the spin multiplicity of the Cr complex with more coronene ligands, namely the spin multiplicity of a bare Cr for B.E.1 and B.E.sum, and the spin multiplicity of the $Cr(pyr)_1^{0/+}$ for B.E.2. When the spin cross-over is taken into account, the multiplicity of the Cr complex with fewer coronene ligands (M´) is set to be its ground spin state predicted by computations. In this study, M´=7 is chosen for Cr atom and $Cr(naph)_1$, and M´= 6 for Cr^+ and $Cr(pyr)_1^+$. B.E.1 values with the spin cross-over (M≠M´) are negative for the neutral complexes in the lower spin states

(M = 1 or 3). This indicates that the flip of the electron spins costs more energy than that released from the formation of the first Cr-coronene bond. The spin cross-over energy also causes the binding energies with the spin conservation rules (M = M´) to be higher than those without, which is observed in Table 6.5.

The binding energies computed for the coronene complexes are compared to those computed for the other PAHs shown in the previous chapters. The B.E.1 values for M = 6 and 7 and the B.E.2 values for M=1 of the Cr-coronene complexes are larger than those of the Cr-benzene complexes according to the calculations. For the cationic Cr-coronene complexes, the B.E.2 values are almost the same as those for the $Cr(bz)_2^+$. This result agrees with the conclusion made from the previous photodissociation study that coronene binds to transition metals stronger than benzene.[5] The B.E.1 values for the $Cr(cor)_1^+$ increase as the conjugated π systems get bigger until coronene. This is probably due to the fact that a more delocalized π system can stabilize the positive charge in to larger degree. However, the B.E.1 values for the neutral complexes (M = 7) do not follow this trend. PBE and M06L predict that pyrene complexes have the B.E.1 (M = 7) values and the B.E.2 (M = 2) values. Both B3LYP and PBE agree that the pyrene complexes have the highest B.E.2 (M = 1) values. These results contradict the proposition of the ligand-exchange experiments that the binding strength of Cr to the arene follows the order of benzene > naphthalene > pyrene.[13,14] If the π-π interaction is the major factor determining the energy, we would expect the B.E.2 of the coronene complex to be larger than those of all the other Cr-PAH complexes. However, the peripheral ring of coronene has the least aromatic index among the PAHs studied here. According to the formula proposed by Balaban and coworkers, a carbon atom shared by one, two, and three rings contribute 1, 1/2, and 1/3 π electron to each ring.[15] So that the aromatic indices of the rings of benzene, naphthalene, pyrene (α), and coronene

(peripheral) are 6π, 5π, 4.33π, and 3.67π, respectively. As a result, benzene has the largest π electron density and coronene has the least. If this were the major consideration, the Cr should bind to benzene stronger than to the other PAHs. The two factors, namely the π-π interaction and the aromaticity, may work against each other and make the energy change not consistent with the size change of the conjugated π system.

Another trend which is noticeable in Table 6.5 is that coronene binds stronger to the Cr in the lower spin state for neutral and cationic complexes respectively. The higher the spin state is, the more unpaired electrons there are in the valence shell. Thus there are fewer unoccupied d orbitals in the Cr in the higher spin state that are available for back donation from the π system. That is why the complexes in the lower spin states usually have lower relative energies. The binding energies B.E.1 and B.E.2 of the cationic complexes are usually higher than those of the corresponding neutral complexes ($\Delta M = \pm 1$), except for the singlet complexes. This indicates that the coronene binds stronger to the Cr^+ cation than to the Cr atom. Therefore, we can conclude that the electrostatic interaction plays an role in the stability of the complexes although it does not significantly affect the Cr-coronene bond distance.

Table 6.5 Bond energies (kcal/mol) of Cr binding to the first (B.E.1), the second (B.E.2), and both (B.E.sum) coronene molecules, with (M≠M') and without (M=M') spin cross-over. B.E.x = $E[Cr(cor)_{x-10/+}] + E[cor] - E[Cr(cor)_{x0/+}]$. B.E.sum = $E[Cr_{0/+}] + 2E[cor] - E[Cr(cor)_{20/+}]$.

		B.E.1		B.E.2		B.E.sum	
	M'	M=M'	M≠M'	M=M'	M≠M'	M=M'	M≠M'
B3LYP	1	55.6	-19.6	75.9	15.9	131.5	26.4
	3	17.7	-32.8	54.4	11.2	72.1	21.6
	5	27.4	-5.0	43.5	28.1	70.9	38.5
	7	10.4	-	21.7	-	32.1	-
	2	58.7	3.6	74.5	27.3	133.1	78.0
	4	90.2	18.0	62.1	29.4	152.3	80.1
	6	50.7	-	53.8	-	104.5	-
PBE	1	95.9	-22.2	82.2	53.5	177.2	59.1
	3	39.8	-17.8	70.7	46.4	110.5	52.9
	5	28.4	0.5	40.3	34.3	73.9	46.0
	7	5.3	-	27.8	-	35.1	-
	2	81.6	22.9	91.3	58.7	172.9	114.2
	4	77.1	36.3	70.0	50.7	147.0	106.3
	6	55.5	-	52.2	-	107.8	-
M06L	1	87.6	-22.6	81.8	52.1	169.4	59.1
	3	34.2	-16.1	70.4	47.3	104.6	54.4
	5	18.6	4.8	45.9	43.6	64.5	50.7
	7	7.0	-	40.1	-	47.2	-
	2	77.6	17.2	89.4	50.6	166.9	106.6
	4	75.5	34.1	71.4	49.6	146.9	105.5
	6	56.0	-	58.3	-	114.3	-

Ionization Potentials

The calculated vertical and adiabatic ionization potentials (IP_v and IP_a) are presented in Table 6.6. The selection rule for the electron multiplicity of $\Delta M = \pm 1$ is applied for vertical ionizations here. For vertical ionization, the structures of cations are inherited from the neutral clusters. Since the lowest energy computed by B3LYP for the neutral $Cr(cor)_2$ is a quintet, the IP_a is evaluated as the M=6←5 transition. In the same manner, the IP_a of $Cr(cor)_2$ computed by B3LYP is evaluated as the M=6←1 transition. The ionization potentials of $_{6\leftarrow7}Cr(cor)_1$ and $_{2\leftarrow1}Cr(cor)_2$ are smaller than those of the corresponding Cr-pyrene complexes, and are thus also smaller than those of the corresponding Cr-naphthalene and Cr-benzene complexes. This is probably because coronene has a larger conjugated π system to delocalize the positive charge, thus making the cations more stable.

Summary

In the Cr-coronene complexes, the Cr has a slight preference to bind to the peripheral ring of coronene (*b*, *c*, or *d*). The energy differences between the structures differing by where the Cr atoms bind are small. On the other hand, the staggering angle between the two coronene molecules makes a significant difference on the relative energies, which means the π-π interaction is an important component of the Cr-coronene bond. All three DFT methods used in this study predict the ground spin states of the $Cr(cor)_{1}^{0/+}$ complexes to be the highest spin states, namely the septet and the sextet. However, they disagree on the ground states for the $Cr(cor)_{2}^{0/+}$ complexes. The Cr-ring distances vary with the spin multiplicities as the other PAH complexes do. Hence in the sandwich structures of the $Cr(cor)_{2}^{0/+}$ complexes, the two coronenes are not parallel, but are tilted towards or away from the Cr depending on the spin state. The computed

binding energies shown in this study are in agreement with the previous experiment that coronene binds stronger to transition metals than benzene does. The complexes in higher spin states have lower Cr-PAH binding energies, which means the d-π interaction is involved in the bonds. By comparing the binding energies of coronene and those of the other PAHs to the Cr, we can deduce that not only the size of the conjugated π system matters, but also does the π electron density of the ring to which the Cr binds. The ionization potentials demonstrate that the larger conjugated π system gives the cationic Cr-coronene complexes more stability compared to the other PAH complexes.

Table 6.6 Vertical ionization potentials (IP_v) and adiabatic ionization potentials (IP_a) of $Cr(cor)_x$ complexes in the unit of eV, where the spin multiplicity change is limited to $\Delta M=\pm 1$ in vertical ionizations. M is the spin multiplicity of a neutral complex, and M´ is the spin multiplicity of a cationic complex.

			PBE		B3LYP		M06L	
Complex	M	M'	IP_v	IP_a	IP_v	IP_a	IP_v	IP_a
	1	2	5.44		4.93		5.30	
	3	2	5.54		5.67		5.46	
x=1	3	4	5.05		4.85		4.70	
	5	4	6.08		6.13		5.73	
	5	6	5.25		4.58		4.85	
	7	6	5.41	5.14	5.46	5.20	5.00	5.14
	1	2	4.94	4.91	4.80		4.81	4.44[a]
	3	2	4.74		4.70		4.72	
x=2	3	4	5.09		4.56		4.78	
	5	4	4.80		5.34		4.88	
	5	6	4.82		4.27	4.08	4.34	
	7	6	4.16		3.98		4.05	

[a] M=1 and M'=6.

References

(1) Dunbar, R. C.; Uechi, G. T.; Asamoto, B. Radiative Association Reactions of Silicon and Transition-Metal Cations with the PAH Compounds Benzene, Naphthalene, and Anthracene. *J. Am. Chem. Soc.* **1994**, *116*, 2466–2470.

(2) Ho, Y.-P.; Yang, Y.-C.; Klippenstein, S. J.; Dunbar, R. C. Binding Energies of Ag^+ and Cd^+ Complexes from Analysis of Radiative Association Kinetics. *J. Phys. Chem. A* **1997**, *101*, 3338–3347.

(3) Foster, N. R.; Grieves, G. A.; Buchanan, J. W.; Flynn, N. D.; Duncan, M. A. Growth and Photodissociation of Cr_x-$(Coronene)_y$ Complexes. *J. Phys. Chem. A* **2000**, *104*, 11055–11062.

(4) Ayers, T. M.; Westlake, B. C.; Duncan, M. A. Laser Plasma Production of Metal and Metal Compound Complexes with Polycyclic Aromatic Hydrocarbons. *J. Phys. Chem. A* **2004**, *108*, 9805–9813.

(5) Buchanan, J. W.; Grieves, G. A.; Reddic, J. E.; Duncan, M. A. Novel Mixed Ligand Sandwich Complexes: Competitive Binding of Iron with Benzene, Coronene, and C_{60}. *Int. J. Mass Spectrom.* **1999**, *182–183*, 323–333.

(6) Dunbar, R. C. Binding of Transition-Metal Ions to Curved π Surfaces: Corannulene and Coronene. *J. Phys. Chem. A* **2002**, *106*, 9809–9819.

(7) Senapati, L.; Nayak, S. K.; Rao, B. K.; Jena, P. Atomic Structure, Binding Energy, and Magnetic Properties of Iron Atoms Supported on a Polyaromatic Hydrocarbon. *J. Chem. Phys.* **2003**, *118*, 8671–8680.

(8) Philpott, M. R.; Kawazoe, Y. Bonding and Magnetism in Transition Metal Sandwich Structures with the Aromatic Hydrocarbon Coronene $C_{24}H_{12}$ Outer Layers. *Chem. Phys.*

2007, *342*, 223–235.

(9) Türker, L.; Gümüs, S. DFT Studies on η6-Coronene-Cr(CO)3 Complexes. *Acta Chim. Slov.* **2009**, *56*, 246–253.

(10) Lao, K. U.; Tsou, P. K.; Lankau, T.; Yu, C. H. A Computational Study of Organic Polyradicals Stabilized by Chromium Atoms. *Phys. Chem. Chem. Phys.* **2012**, *14*, 138–147.

(11) Dougherty, D. A. Cation-π Interactions in Chemistry and Biology: A New View of Benzene, Phe, Tyr, and Trp. *Science* **1996**, *271*, 163–168.

(12) Wigner, E.; Witmer, E. E. Über Die Struktur Der Zweiatomigen Molekelspektren Nach Der Quantenmechanik. *Zeitschrift für Phys.* **1928**, *51*, 859–886.

(13) Howell, J. A. S.; Ashford, N. F.; Dixon, D. T.; Kola, J. C.; Albright, T. A.; Kang, S. K. The Arene-Exchange Reaction in Naphthalene- and Pyrene-Cr(CO)3. *Organometallics* **1991**, *10*, 1852–1864.

(14) Bush, B. F.; Lynch, V. M.; Lagowski, J. J. Transition-Metal Organometallic Compounds: 8: Arene Exchange Reactions of Bis(Naphthalene)Chromium. *Organometallics* **1987**, *6*, 1267–1275.

(15) Balaban, A. T.; Durdević, J.; Gutman, I.; Jeremić, S.; Radenković, S. Correlations between Local Aromaticity Indices of Bipartite Conjugated Hydrocarbons. *J. Phys. Chem. A* **2010**, *114*, 5870–5877.

CHAPTER 7

PRODUCTION OF CHROMIUM-PAH COMPLEXES VIA A LASER VAPORIZATION FLOWTUBE REACTOR

Introduction

Due to their similarity to graphene, polycyclic aromatic hydrocarbons (PAHs) are often studied as models of graphenes.[1–3] Comparably, transition metal-PAH complexes are good prototypes for the study of the transition metal supported on carbon materials. Chromium, an early transition metal from group 6, is especially interesting since it can be coordinated by two six-member carbon rings to meet the 18-electron rule. The pyrene and coronene complexes have been experimentally studied in the gas phase,[4–10] and have been studied by theory as well.[11–16] However, no one has reported the successful synthesis and isolation of the Cr-pyrene and Cr-coronene complexes. This study attempts to synthesize these complexes via the laser vaporization flowtube reactor (LVFR).

Metal-PAH ion complexes have been reported previously in gas-phase experiments using FT-ICR mass spectrometry.[17–19] In those setups, the transition metal ions reacted with the PAH vapors at very low pressures (10^{-9}-10^{-7} torr) The products were detected with mass spectrometers. Duncan and co-workers have produced a variety of metal and multi-metal complexes with PAHs by laser ablating film-coated metal samples in a molecular beam cluster source.[5,8,10,20–23] The PAH vapors are generated by laser ablation. A gas channel employed in their setup increased the probability of collisions between the metal plasma and the PAH vapors. The supersonic expansion was used to cool the ions. The complexes produced in their study

were also detected using mass spectrometry. In later studies, powder mixtures of metals or their compounds and PAHs were desorbed by focused laser beams, and the products were detected in a time-of-flight mass spectrometer without any collisional cooling.[7,24] The successful production of coronene or pyrene complexes with transition metals indicate that the stability of the Cr-pyrene or Cr-coronene complexes is enough to tolerate the hot laser desorption conditions.

The large scale syntheses of the Cr-pyrene and the Cr-coronene complexes are challenging despite the stabilities of the products, just as the preparation of bis(naphthalene)chromium was not reported until two decades after the first bis(benzene)chromium preparation.[25,26] The main difficulty is the low vapor pressure of large PAHs. Benzene is a liquid with a high vapor pressure, so it is relatively easy to make benzene complexes in the gas phase. To make transition metal-naphthalene complexes in a large scale, naphthalene vapor is required in a high concentrations. The case is worse for coronene, since the vapor pressure of coronene at 420 K is about 2×10^{-5} torr, while the vapor pressure of naphthalene at room temperature is about 3×10^{-3} torr.[27]

The LFVR has been used to synthesize several ligand-coated metal or metal oxide clusters in milligram quantities.[28–30] In this study, the LVFR is modified with a ceramic oven to generate PAH vapors. The oven opening is placed near the metal rod to create a concentrated PAH atmosphere around the metal. The details are discussed below.

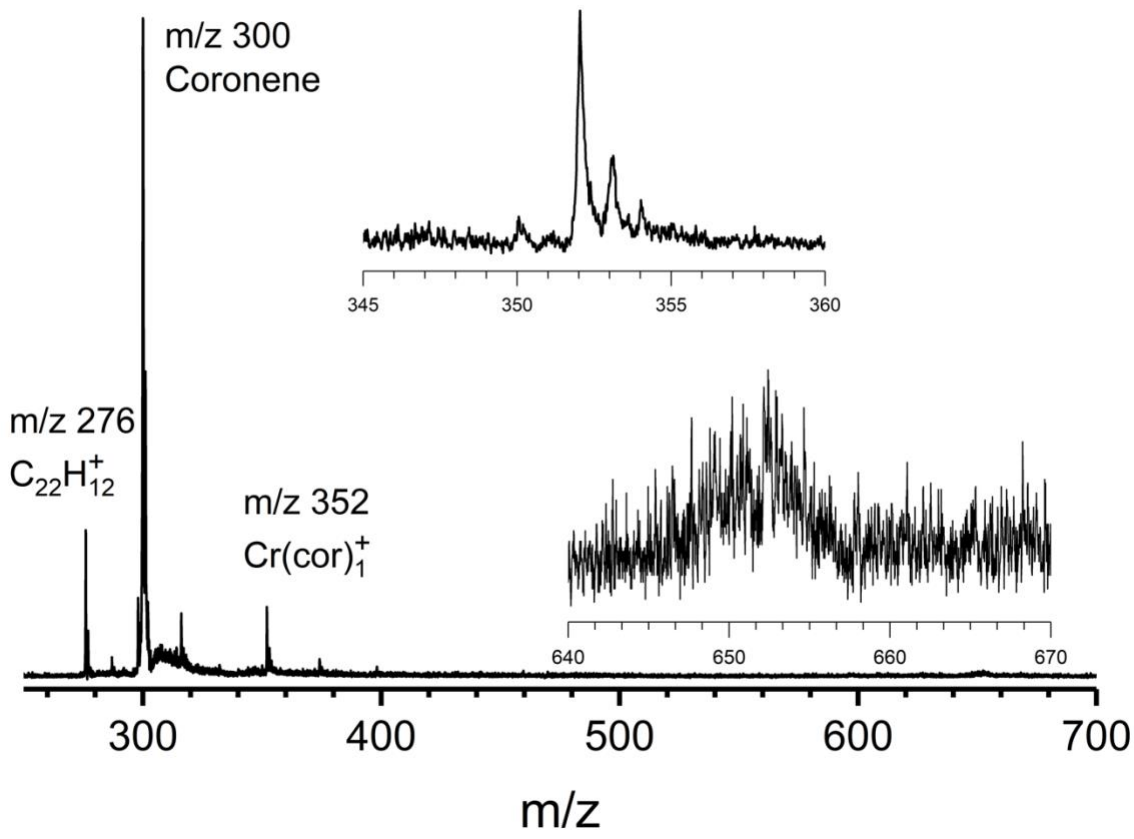

Figure 7.1 Mass spectrum of Cr-coronene produced in the LVFR. The two insets are the zoomed-in regions of this mass spectrum.

Experiment

Details of the LVFR are in Chapter 2. A laser fluence of 120–100 mJ/pulse and a repetition rate of 400 Hz is used to vaporize the chromium rod. The laser is focused to a 1×8 mm rectangular spot on a rotating ¼ inch diameter chromium rod. The higher laser powers and the larger irradiation area facilitate the metal ablation more than the laser sources used in the previous gas-phase experiments.[5,8,10,17–23] A hollow cylindrical ceramic oven is placed next to the metal rod with the opening facing the metal rod. The oven filled with the coronene powder (80% purity) is heated by a nickel-chromium alloy resistance heating wire. The temperature is monitored by a thermocouple attached at the end of the oven. The temperature is controlled to be at about 160ºC. Helium (UHP) at 200 psi is expanded continuously alongside the metal rod through a ~0.8 mm hole positioned about 6 mm away from the rod. The introduction of helium results in an ambient pressure of 10 torr in the flow tube. Argon (UHP) is introduced from the side of the second chamber to increase the pressure by 1×10^{-1} torr in the flow tube. The flowing gas provides collisional cooling and entrains materials in it. The materials coat the first aperture between the first and the second chamber. They are scraped off the surface and loaded onto the copper probe tip for mass spectrometry.

Results and Discussion

The materials collected from the upper side of the aperture have a dark brown color. These materials should be composed of not only the Cr-coronene complexes, but also the unreacted chromium and coronene. Laser desorption mass spectrometry is used for analysis. A mass spectrum of the sample is presented in Figure 7.1. The highest peak in this figure is assigned to coronene (m/z = 300). The peaks that are assigned to chromium (m/z = 52) have similar

abundances as coronene, but they are not shown in this figure. The peaks presented in the upper inset have the highest peak at m/z = 352. By comparing to the isotope pattern of chromium, they can be assigned to $Cr(cor)_1$. In the lower inset, we can see peaks roughly at m/z = 652, which can be assigned to $Cr(cor)_2$. However, the resolution is so low that this assignment is not assured.

In the previous study, the mass spectra of mixed powders of chromium and coronene showed peaks which were assigned to coronene, $Cr(cor)_1$, and $Cr(cor)_2$.[7] The Cr-coronene complexes did not exist until the laser desorption. Consequently, one mass spectrum in Figure 7.1 alone cannot prove that the Cr-coronene complexes are synthesized in the LVFR. Therefore, mass spectra are taken for the mixed chromium and coronene powder in this study to determine if the complexes are collected from the LVFR. Two mass spectra are taken. One sample tip is prepared by pressing and grinding the sample tip on the mixed powders. A thin layer of powders is loaded. A piece of pressed pellet made from the mixed powders is taped on the other sample tip. The pellet is about 0.5 mm thick. These spectra are taken with similar mass spectrometry conditions that are used for the mass spectrum of the synthesized products.

Figure 7.2 shows the mass spectra of the mixed powders of chromium and coronene. Besides peaks that are assigned to coronene, other peaks can be assigned to the known PAH molecules, such as $C_{22}H_{12}$ (m/z = 276), $C_{28}H_{14}$ (m/z = 350), $C_{30}H_{14}$ (m/z = 374) and $C_{32}H_{14}$ (m/z = 398). They are impurities in the coronene powder that also show up in the mass spectra of the coronene from the bottle. However, neither $Cr(cor)_1$ nor $Cr(cor)_2$ peaks are shown in these mass spectra. Through the comparison of the spectra of the mixed powder sample and the synthesized sample, we could conclude that the Cr-coronene complexes are made in the LVFR instead of in the mass spectrometer.

Summary

The LVFR has been successfully used to produce the Cr-coronene complexes. However, the yield is still low (<1 mg collected after two hours of running) and the percentage of the complexes in the products are unknown. Optimizations of the experimental conditions are needed to increase the yield in the future. Additionally, there is not a good way to separate $Cr(cor)_1$ or $Cr(cor)_2$ from the products so far. Hence efforts should be made to purify the samples as well.

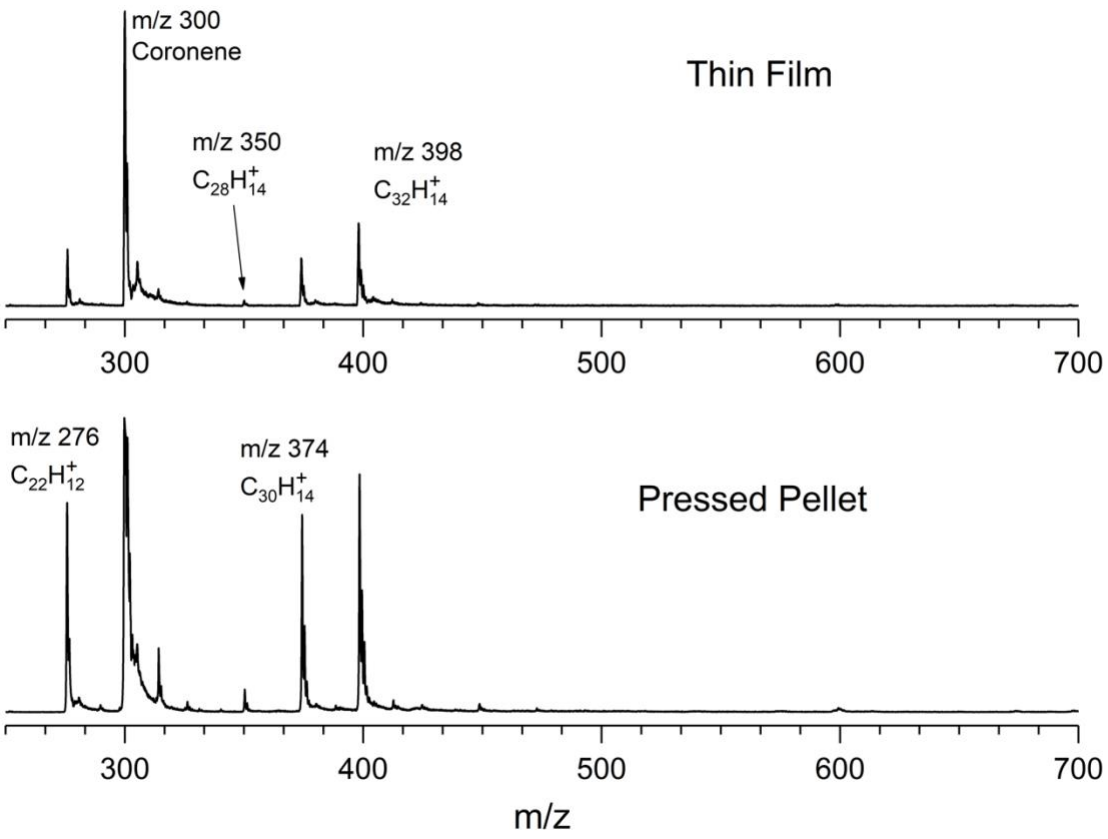

Figure 7.2 Mass spectra of mixed chromium and coronene powders as a thin film and as a pressed pellet.

References

(1) Whittingham, M. S.; Jacobson, A. J. *Intercalation Chemistry*; Academic Press, 1982.

(2) Dresselhaus, M. S.; Dresselhaus, G.; Eklund, P. C. *Science of Fullerenes and Carbon Nanotubes: Their Properties and Applications*; Elsevier Science, 1996.

(3) Enoki, T.; Suzuki, M.; Endo, M. *Graphite Intercalation Compounds and Applications*; Oxford University Press, 2003.

(4) Elustondo, F.; Dalibart, M.; Deroult, J.; Mascetti, J. Matrix Isolation Spectroscopy Study of Iron Reactivity towards PAHs. *Phys. Chem. Earth, Part C Solar, Terr. Planet. Sci.* **1999**, *24*, 583–589.

(5) Foster, N. R.; Grieves, G. A.; Buchanan, J. W.; Flynn, N. D.; Duncan, M. A. Growth and Photodissociation of Cr_x-$(Coronene)_y$ Complexes. *J. Phys. Chem. A* **2000**, *104*, 11055–11062.

(6) Dunbar, R. C. Binding of Transition-Metal Ions to Curved π Surfaces: Corannulene and Coronene. *J. Phys. Chem. A* **2002**, *106*, 9809–9819.

(7) Ayers, T. M.; Westlake, B. C.; Duncan, M. A. Laser Plasma Production of Metal and Metal Compound Complexes with Polycyclic Aromatic Hydrocarbons. *J. Phys. Chem. A* **2004**, *108*, 9805–9813.

(8) Scott, A. C.; Buchanan, J. W.; Flynn, N. D.; Duncan, M. A. Photodissociation of Iron-Pyrene and Iron-Perylene Cation Complexes. *Int. J. Mass Spectrom.* **2007**, *266*, 149–155.

(9) Wang, Y.; Szczepanski, J.; Vala, M. Vibrational Spectroscopy of Neutral Complexes of Fe and Polycyclic Aromatic Hydrocarbons. *Chem. Phys.* **2007**, *342*, 107–118.

(10) Scott, A. C.; Buchanan, J. W.; Flynn, N. D.; Duncan, M. A. Photodissociation Studies of Calcium–Coronene and Calcium–Pyrene Cation Clusters. *Int. J. Mass Spectrom.* **2008**,

269, 55–61.

(11) Senapati, L.; Nayak, S. K.; Rao, B. K.; Jena, P. Atomic Structure, Binding Energy, and Magnetic Properties of Iron Atoms Supported on a Polyaromatic Hydrocarbon. *J. Chem. Phys.* **2003**, *118*, 8671–8680.

(12) Philpott, M. R.; Kawazoe, Y. Bonding and Magnetism in Transition Metal Sandwich Structures with the Aromatic Hydrocarbon Coronene $C_{24}H_{12}$ Outer Layers. *Chem. Phys.* **2007**, *342*, 223–235.

(13) Simon, A.; Joblin, C. Thermochemistry and Infrared Spectroscopy of Neutral and Cationic Iron−Polycyclic Aromatic Hydrocarbon Complexes of Astrophysical Interest: Fundamental Density Functional Theory Studies. *J. Phys. Chem. A* **2007**, *111*, 9745–9755.

(14) Türker, L.; Gümüs, S. DFT Studies on η_6-Coronene-$Cr(CO)_3$ Complexes. *Acta Chim. Slov.* **2009**, *56*, 246–253.

(15) Lao, K. U.; Tsou, P. K.; Lankau, T.; Yu, C. H. A Computational Study of Organic Polyradicals Stabilized by Chromium Atoms. *Phys. Chem. Chem. Phys.* **2012**, *14*, 138–147.

(16) Ding, L.-P.; Kuang, X.-Y.; Shao, P.; Zhong, M.-M. Evolution of Structure and Properties of Neutral and Negatively Charged Transition Metal–Coronene Complexes: A Comprehensive Analysis. *Dalt. Trans.* **2013**, *42*, 8644–8654.

(17) Dunbar, R. C.; Uechi, G. T.; Asamoto, B. Radiative Association Reactions of Silicon and Transition-Metal Cations with the PAH Compounds Benzene, Naphthalene, and Anthracene. *J. Am. Chem. Soc.* **1994**, *116*, 2466–2470.

(18) Pozniak, B. P.; Dunbar, R. C. Monomer and Dimer Complexes of Coronene with Atomic Ions. *J. Am. Chem. Soc.* **1997**, *119*, 10439–10445.

(19) Szczepanski, J.; Wang, H.; Vala, M.; Tielens, A. G. G. M.; Eyler, J. R.; Oomens, J. Infrared Spectroscopy of Gas-Phase Complexes of Fe^+ and Polycyclic Aromatic Hydrocarbon Molecules. *Astrophys. J.* **2006**, *646*, 666–680.

(20) Buchanan, J. W.; Reddic, J. E.; Grieves, G. A.; Duncan, M. A. Metal and Multimetal Complexes with Polyaromatic Hydrocarbons: Formation and Photodissociation of Fe_x-$(Coronene)_y$ Cations. *J. Phys. Chem. A* **1998**, *102*, 6390–6394.

(21) Buchanan, J. W.; Grieves, G. A.; Reddic, J. E.; Duncan, M. A. Novel Mixed Ligand Sandwich Complexes: Competitive Binding of Iron with Benzene, Coronene, and C_{60}. *Int. J. Mass Spectrom.* **1999**, *182–183*, 323–333.

(22) Foster, N. R.; Buchanan, J. W.; Flynn, N. D.; Duncan, M. A. Ring Destruction and Carbide Formation in Niobium-PAH Complexes. *Chem. Phys. Lett.* **2001**, *341*, 476–482.

(23) Duncan, M. A.; Knight, A. M.; Negishi, Y.; Nagao, S.; Judai, K.; Nakajima, A.; Kaya, K. Photoelectron Spectroscopy of $V_x(Coronene)_y$ and $Ti_x(Coronene)_y$ Anions. *J. Phys. Chem. A* **2001**, *105*, 10093–10097.

(24) Ayers, T. M.; Westlake, B. C.; Preda, D. V.; Scott, L. T.; Duncan, M. A. Laser Plasma Production of Metal−Corannulene Ion−Molecule Complexes. *Organometallics* **2005**, *24*, 4573–4578.

(25) Elschenbroich, C.; Möckel, R. Bis(η^6-naphthalene)Chromium(0). *Angew. Chemie Int. Ed.* **1977**, *16*, 870–871.

(26) Kündig, E. P.; Timms, P. L. Metal Atom Preparation and Ligand Displacement Reactions of Bisnaphthalenechromium and Related Compounds. *J. Chem. Soc., Chem. Commun.* **1977**, 912–913.

(27) Oja, V.; Suuberg, E. M. Vapor Pressures and Enthalpies of Sublimation of Polycyclic

Aromatic Hydrocarbons and Their Derivatives. *J. Chem. Eng. Data* **1998**, *43*, 486–492.

(28) Ayers, T. M.; Fye, J. L.; Li, Q.; Duncan, M. A. Synthesis and Isolation of Titanium Metal Cluster Complexes and Ligand-Coated Nanoparticles with a Laser Vaporization Flowtube Reactor. *J. Clust. Sci.* **2003**, *14*, 97–113.

(29) Ard, S.; Dibble, C. J.; Akin, S. T.; Duncan, M. A. Ligand-Coated Vanadium Oxide Clusters: Capturing Gas-Phase Magic Numbers in Solution. *J. Phys. Chem. C* **2011**, *115*, 6438–6447.

(30) Akin, S. T.; Liu, X.; Duncan, M. A. Laser Synthesis and Spectroscopy of Acetonitrile/Silver Nanoparticles. *Chem. Phys. Lett.* **2015**, *640*, 161–164.